JGR Solid Earth

RESEARCH ARTICLE
10.1029/2022JB025687

The Sub-Ice Structure of Mt. Melbourne Volcanic Field (Northern Victoria Land, Antarctica) Uncovered by High-Resolution Aeromagnetic Data

Alessandro Ghirotto[1], Egidio Armadillo[1], Laura Crispini[1], Andrea Zunino[2], Fabio Caratori Tontini[1], and Fausto Ferraccioli[3,4]

[1]DISTAV, University of Genova, Genova, Italy, [2]Institute of Geophysics, ETH Zürich, Zürich, Switzerland, [3]Istituto di Oceanografia e Geofisica Sperimentale - OGS, Sgonico, Italy, [4]British Antarctic Survey, Cambridge, UK

Key Points:

- First detailed geophysical model of the internal structure of the Mt. Melbourne Volcanic Field
- Magnetic anomalies and rock magnetism data suggest the field is predominantly built-up by reversely-polarized volcanics
- Our results support an establishment of the Mt. Melbourne edifice at least at the reverse polarity Matuyama magnetic epoch

Supporting Information:

Supporting Information may be found in the online version of this article.

Correspondence to:

A. Ghirotto and E. Armadillo,
alessandro.ghirotto@edu.unige.it;
egidio.armadillo@unige.it

Citation:

Ghirotto, A., Armadillo, E., Crispini, L., Zunino, A., Caratori Tontini, F., & Ferraccioli, F. (2023). The sub-ice structure of Mt. Melbourne Volcanic Field (Northern Victoria Land, Antarctica) uncovered by high-resolution aeromagnetic data. *Journal of Geophysical Research: Solid Earth*, *128*, e2022JB025687. https://doi.org/10.1029/2022JB025687

Received 26 SEP 2022
Accepted 4 JUL 2023

Author Contributions:

Conceptualization: Alessandro Ghirotto, Egidio Armadillo
Data curation: Alessandro Ghirotto
Formal analysis: Alessandro Ghirotto
Funding acquisition: Egidio Armadillo, Laura Crispini
Investigation: Alessandro Ghirotto, Egidio Armadillo
Methodology: Alessandro Ghirotto, Egidio Armadillo, Andrea Zunino

Abstract The Mt. Melbourne Volcanic Field is a quiescent volcanic complex located in Northern Victoria Land, Antarctica, mostly covered by ice. Its inner structure has remained largely unknown, due to the paucity of outcrops and the lack of detailed multi-disciplinary investigations. Here we present a novel high-resolution aeromagnetic dataset, revealing strong long-wavelength negative anomalies superimposed by short-wavelength positive ones forming characteristic radial patterns. Automatic lineament detection, through the Hough transform technique applied to the tilt derivative of our magnetic dataset, shows prevailing NW-SE-to NNE-SSW-trending structural features, which combined with the few structural field observations contribute to define the deformation pattern. Pre-existing and novel magnetic property measurements, coupled with available geochronological data, are used to constrain a two-step 3D magnetic inversion. A layer-structured Oldenburg-Parker's inversion was utilized to model the deep and long-wavelength components of the magnetic field, whereas a linear inversion based on a set of shallower prisms was used to model the short-wavelength components. The final 3D model shows widespread reversely-polarized volcanics, which are locally intruded and superimposed, respectively by swarms of normally-polarized dikes and radial lava flows along paleo-valleys. These results support the onset of volcanic activity in the entire field at least in the Matuyama magnetic epoch, that is, between 2.58 and 0.78 Ma.

Plain Language Summary Airborne high-resolution magnetic data play a crucial role in the understanding of the geological structure of ice-buried volcanoes. In fact, an interesting property of magnetic minerals contained in volcanic rocks is that of retaining, after cooling below a certain characteristic temperature (i.e., Curie temperature), a permanent magnetization called remanent. Its direction (polarization) at the South Pole can be normal if rocks are cooled when the Earth's magnetic field presents negative inclination (as the current Brunhes epoch), whereas reverse in the case the Earth's magnetic field shows positive inclination (i.e., the Earth's magnetic field poles swap places). As a consequence, at polar latitudes, positive magnetic anomalies are associated with normally-polarized rocks and, conversely, negative anomalies with reversely-polarized rocks. Thanks to this property, in this study we have carried out the first reconstruction of the internal architecture of the Mt. Melbourne Volcanic Field. Our results, constrained by independent geological and geophysical information, suggest the volcanic complex is composed mainly by an older reversely-polarized unit superimposed and intruded locally by younger normally-polarized lava flows. Being the periods of magnetic polarity reversal well known, we have been able to estimate the beginning of a widespread volcanic activity before the last Brunhes-Matuyama polarity reversal.

1. Introduction

Antarctica represents the last frontier in Earth geological exploration, where the thick ice sheet mostly prevents direct observation of the subglacial geology and tectonics affecting the continent. In this context, half a century of aeromagnetic investigations have offered a significant way to image structures, lithologies and volcanic features buried beneath the ice sheet, helping scientists to study the geological framework of the entire continent (e.g., Ebbing et al., 2021; Ferraccioli et al., 2005, 2009a,b; Goodge & Finn, 2010; Golynsky et al., 2018; Jordan et al., 2022; Kim et al., 2022). Only few high-resolution aeromagnetic datasets (HRAM) are available in Antarctica (e.g., Armadillo et al., 2012; Damaske et al., 2014; Ferraccioli et al., 2005; Ghidella et al., 2013; Jordan et al., 2014; Mieth et al., 2014; Ruppel et al., 2017; Wilson et al., 2007), which allowed the investigation of

Project Administration: Egidio Armadillo
Resources: Egidio Armadillo
Software: Alessandro Ghirotto, Egidio Armadillo, Andrea Zunino
Supervision: Egidio Armadillo, Laura Crispini, Andrea Zunino
Validation: Alessandro Ghirotto, Egidio Armadillo, Laura Crispini, Andrea Zunino, Fabio Caratori Tontini, Fausto Ferraccioli
Visualization: Alessandro Ghirotto
Writing – original draft: Alessandro Ghirotto

specific areas of geological interest to be carried out in greater detail. A HRAM survey in a volcanic environment, for example, is fundamental not only to reveal the interior of the volcanic edifice but also to map the magmatic pattern, including alteration related to hydrothermal activity, and the volcano-tectonic deformation setting, with important implications for contributing to the reconstruction of the volcanic history (e.g., Bouligand et al., 2014; Finn et al., 2007; Finn et al., 2022; Finn & Morgan, 2002).

A site of particular interest where a novel HRAM is available is the sub-ice Mt. Melbourne Volcanic Field (MVF), a quiescent volcanic complex located in Northern Victoria Land whose most recent volcanic activity is estimated between 1862 and 1922 (Lyon, 1986). This field, placed between the Transantarctic Mountains rift shoulder and the western side of the West Antarctic Rift System (WARS) (Figure 1a), is considered to have the potential for future large-scale explosive eruptions (Giordano et al., 2012). However, despite a variety of geological, geochemical and geophysical investigations performed to improve the knowledge of the MVF and assess its hazard (Adamson & Cavaney, 1967; Armstrong, 1978; Armienti et al., 1988; Armienti et al., 1991; Beccaluva, Coltorti, et al., 1991; Beccaluva, Civetta, et al., 1991; Bonaccorso et al., 1995; Bonaccorso et al., 1996; Cremisini et al., 1991; Del Carlo et al., 2022; Ferraccioli et al., 2000; Gambino et al., 2016; Gambino et al., 2021; GANOVEX Team, 1987; Giordano et al., 2012; Gubellini & Postpischl, 1991; Hörnig et al., 1991; Keys et al., 1983; Lanzafame & Villari, 1991; Lanza et al., 1991; Lee et al., 2015; Lyon, 1986; Lyon & Giggenbach, 1974; Manzoni & Miletto, 1988; Müller et al., 1991; Nathan & Schulte, 1967, 1968; Pasquale et al., 2009; Vignaroli et al., 2015; Wörner & Viereck, 1987, 1989; Wörner et al., 1989), there is no clear consensus on its geological structure and temporal evolution. The main reason is that ice covers most of the volcano, limiting the data collection to small, scattered areas of geological outcrops which prevent a detailed characterization of the volcanic area.

The aim of this study is the geophysical characterization of the MVF. In Section 2 we give an overview of the geological and structural setting of the volcanic complex, whereas in Section 3 we present the analysis and enhancement of the novel HRAM dataset, interpreted along with geochronological and both unedited and available magnetic susceptibility and remanence data collected by authors over the MVF during different Italian Antarctic expeditions of the PNRA (Italian National Antarctic Research Program). In Section 4, magnetic patterns of subglacial volcanic deposits are imaged with unprecedented detail by means of two complementary inversion methods, thanks to which in Section 5 we improve noteworthy the general knowledge of the volcanic history of the MVF. In addition, the methodologies used and the procedures followed in this study may represent a valid operating model to investigate other remote volcanic areas in Antarctica and elsewhere.

2. Geological Framework

The MVF is part of the Mt. Melbourne Volcanic Province (Kyle, 1990; Kyle & Cole, 1974), that extends northward to include the older volcanic centers of Mt. Overlord, Mt. Rittmann, the Pleiades and Malta Plateau (Armadillo et al., 2007; Kyle & Cole, 1974; Kyle, 1990; Smellie & Rocchi, 2021; see Figure 1a). This province belongs to the McMurdo Volcanic Group (Harrington, 1958; Kyle, 1990; Kyle & Cole, 1974), one of the most extensive alkali volcanic provinces in the world, also including the Hallett and the Erebus Volcanic Provinces, respectively northward and southward. The oldest volcanic activity associated with the McMurdo Volcanic Group has been identified in the Meander Intrusives, a 48–18 Ma old set of limited and scattered intrusions exposed on the steep side of the TAM overlooking the Ross Sea and cropping out in the northernmost sector of the MVF (Armienti et al., 1988; GANOVEX Team, 1987; Müller et al., 1991; Tonarini et al., 1997; Pertusati et al., 2012; see Figure 1b).

At a regional scale, the widespread alkaline magmatism comprising the McMurdo Volcanic Group, resting on the crystalline basement of the Ross Orogen Wilson Terrane (Carmignani et al., 1987), is inferred to be related to the opening of the WARS in the Eocene time and its subsequent extension which is still in progress (Lanzafame & Villari, 1991; Rocchi et al., 2002; Roland & Tessensohn, 1987; Salvini et al., 1997; Smellie & Rocchi, 2021). Several authors suggested the regional rifting of the Ross Sea and the uplift of the TAM have affected, at a local scale, the tectonic processes and magmatism of the MVF. Lanzafame and Villari (1991) proposed the localization of the volcanic activity forming MVF could be related to two main intersecting sets of extensional faults striking NW-SE and NNE-SSW, whereas Vignaroli et al. (2015) indicated three main sets of high-angle fault systems trending NW-SW, NE-SW and N-S (Figure 1b). This tectonic setting is inferred to be the consequence of a deformation regime transition (in space and time) from pure transcurrent to extensional in an overall context of oblique rifting affecting the entire Northern Victoria Land (Vignaroli et al., 2015).

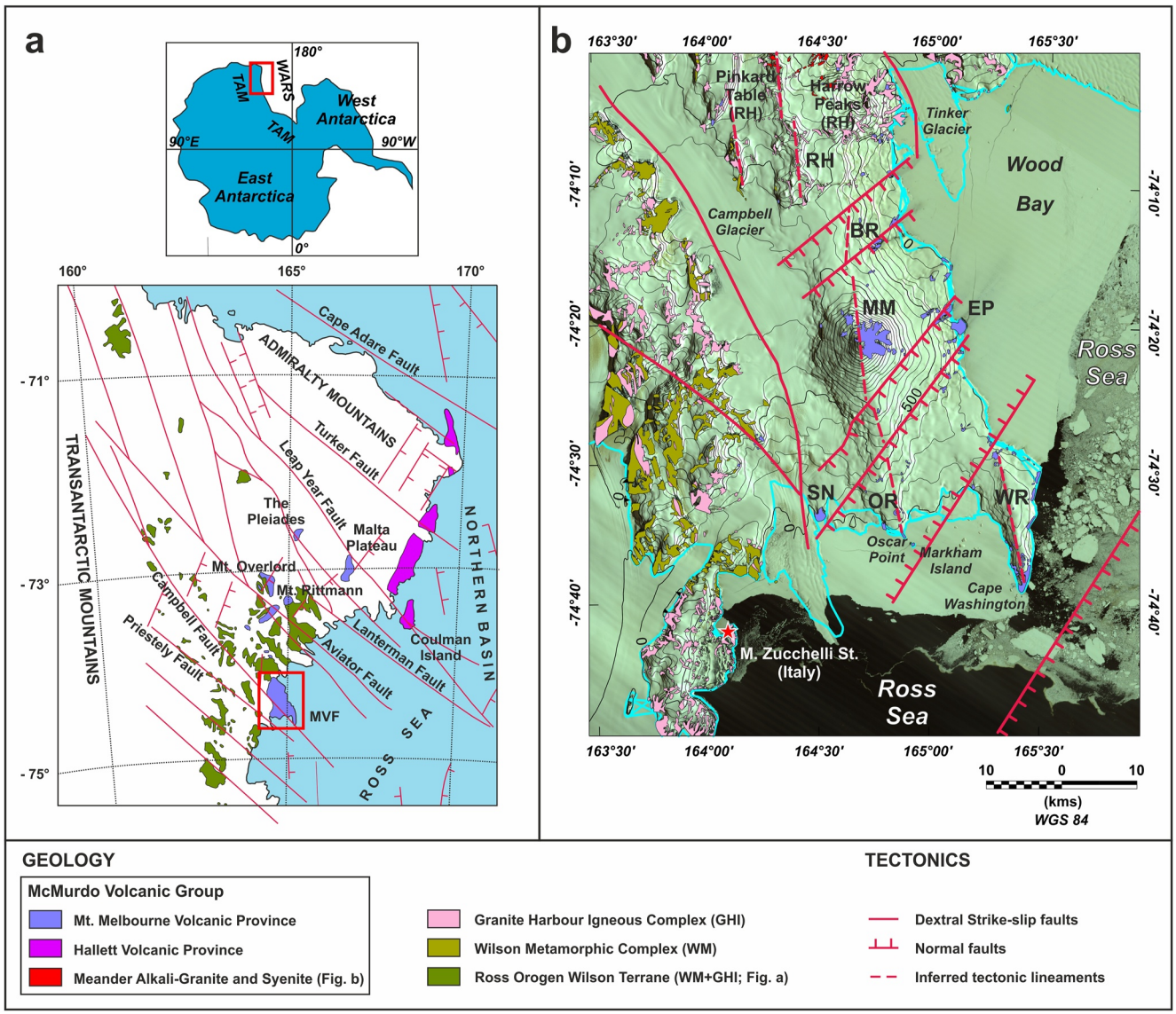

Figure 1. (a) Regional map of the geology and tectonics of Northern Victoria Land (after GANOVEX Team, 1987; Salvini et al., 1997; Storti et al., 2008). (b) Landsat image of the MVF, the study area, with superimposed the recognized geological outcrops and tectonic features affecting the volcanic complex. Contour line intervals every 100 m. Geological and structural data are digitized from Pertusati et al. (2012) and Giordano et al. (2012), Vignaroli et al. (2015), respectively, whereas Landsat image is from Bindschadler et al. (2008). Sub-suites are defined according to Wörner and Viereck (1989) and Pasquale et al. (2009): Washington Ridge (WR), Oscar Ridge (OR), Shield Nunatak (SN) at south, Edmonson Point (EP) at East, Baker Rocks (BR), Random Hills (RH) at north and the Mt. Melbourne volcano (MM). The red star indicates the location of the Italian Antarctic station "Mario Zucchelli".

The MVF is composed of up to 60 scattered subglacial and subaerial volcanic centers surrounding the 2700m-high Mt. Melbourne stratovolcano, subdivided in seven main volcanic sub-suites on the basis of their morphology, eruptive styles and petrography (Wörner & Viereck, 1989; see Figure 1b for their names and acronyms). Wörner and Viereck (1989) proposed the first phase of volcanic activity started about 2.7 Ma at WR and then focused on the MM during the late Pleistocene-Holocene (geochronological data from Armstrong, 1978; Kreuzer 1988-unpubl. report quoted in Wörner & Viereck, 1989). On the other hand, Giordano et al. (2012) proposed new ages for the MVF, postponing the initial development of the MM and its closest peripheral centers to after ~450 ka, in apparent disagreement with both some geochronological data from Lee et al. (2015) and from previous studies (e.g., Armienti & Baroni, 1999; Armienti et al., 1991; Armstrong, 1978; Müller et al., 1991). A comprehensive review of all age estimates published in literature is given by Smellie and Rocchi (2021).

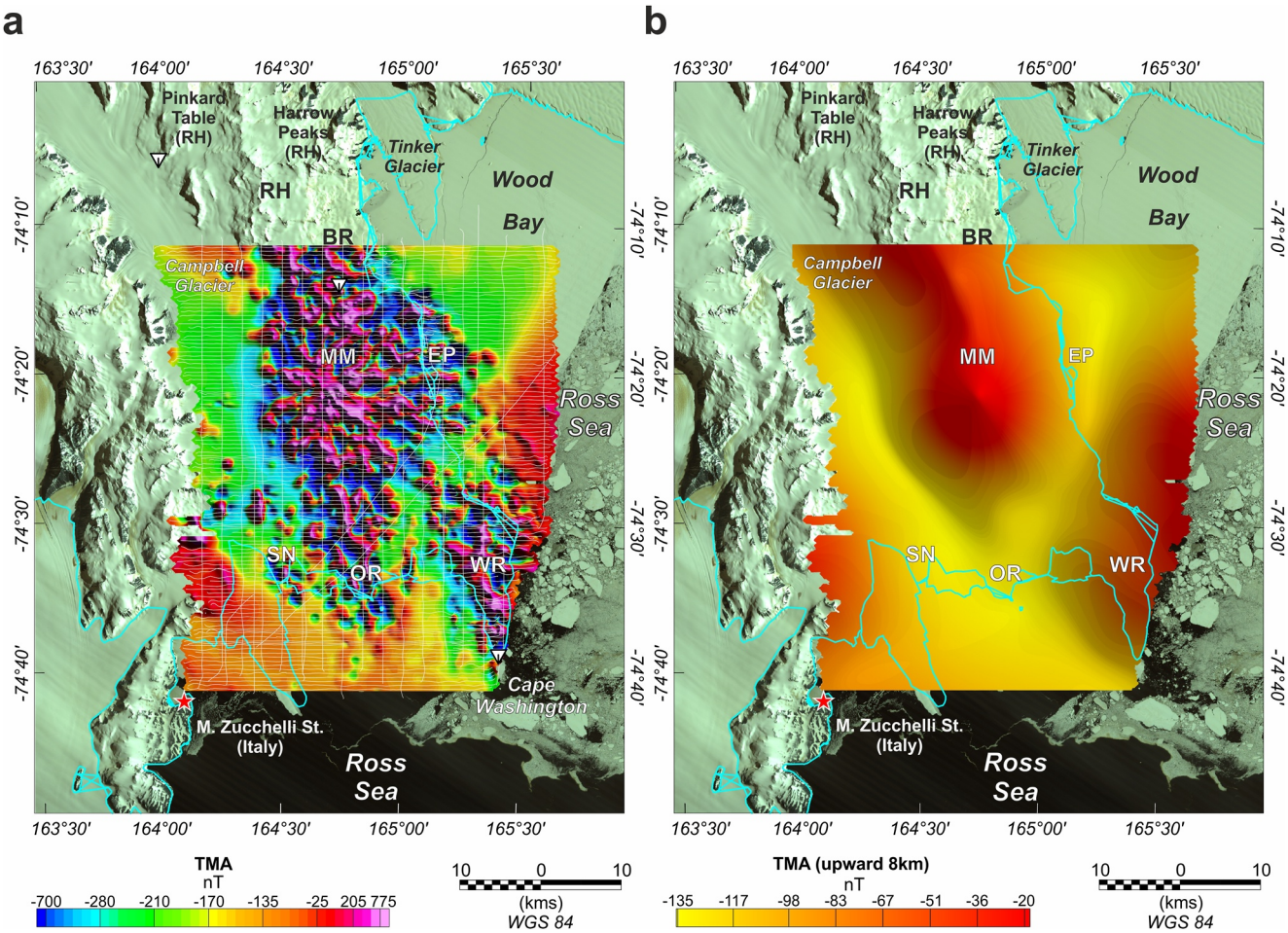

Figure 2. (a) Landsat image with superimposed new High-resolution Total-field Magnetic intensity Anomaly (TMA) data covering the entire MVF. The three inverted white triangles represent the locations of the geomagnetic stations installed during the aeromagnetic survey to monitor the geomagnetic activity. (b) TMA data upward-continued at 8 km height. This low-pass filtered data shows clearly along the entire MVF a pronounced negative anomaly, whereas the positive radial pattern visible in (a) gives way to mild positive anomalies on MM and WR. For abbreviations and other symbols see caption of Figure 1.

However, it is important to outline that most of the existing geochronological data are not always supported by precise sampling localities or sample descriptions. In addition, age estimates refer to scattered sites of subaerial recent lavas, so they do not reflect the likely older completely hidden inner part of the MVF. Therefore, part of the story and architecture of this volcanic complex could be still partially unknown and hidden under the ice.

3. Geophysical Data

In the first part of this Section, we present the technical information about the acquisition and processing of the HRAM data. An innovative technique for automatic magnetic lineament detection gave detailed information about the structural features affecting the MVF. In the second part we present new magnetic susceptibility measurements (listed in Table S1 in Supporting Information S1), integrated with pre-existing magnetic properties data. At the end, we combine all available information, developing a hypothesis about the internal structure of the volcanic complex to be tested through magnetic inversion presented in Section 4.

3.1. HRAM Survey

3.1.1. Data Acquisition & Processing

The HRAM dataset was acquired over a survey area of 2,640 km^2 along 128 lines flown using a Squirrel-B2 helicopter. Line spacing was 500 m and tie intervals 2500 m for a total of 6,490 line km (Figure 2a). The survey was

flown in a draped mode with nominal mean clearance of 450 m from the topographic surface (minimum 235 m, maximum 770 m) monitored using at the same time a radar, a laser (ADM Geophysical Altimeter OPTEC) and a barometric (Rosemount) altimeter. Magnetic data were collected at sampling frequency of 10 Hz using an optically pumped Scintrex MAC III Cesium magnetometer with a resolution of 0.01 nT, installed in a bird configuration. Three geomagnetic base stations, acquiring data at a 30 s sampling rate, were set up at Baker Rocks (BR), Cape Washington and Pinkard Table in order to monitor the Geomagnetic activity prior and during the survey (Figure 2a). A GNSS differential navigation system (Magnavox 4200 + GPS Trimble ProXRS) was used to allow for differential corrections to be applied to the positioning data.

The processing of raw magnetic data has been carried out according to classical aero-geophysical procedures (e.g., Luyendyk, 1997). In detail, initial raw data check was performed in the field and any plausible artifacts or spikes were removed. Lag correction was applied to correct for the relative positioning between the helicopter GPS antenna and the magnetic sensor (about 15 m) during flights, and diurnal variations of the Geomagnetic field were subtracted using base stations magnetic data recordings. The positional data were recovered using carrier-phase, continuous, kinematic GPS processing techniques (Mader, 1992). The geomagnetic reference field for all the data points of the survey, calculated using the proper DGRF coefficients, was then subtracted to obtain Total-field Magnetic intensity Anomaly (TMA) data. Residual diurnal magnetic variations errors in the data were removed using leveling procedures, whereas residual flight line-related corrugation noise was minimized by means of micro-leveling techniques (Ferraccioli et al., 1998). TMA data have not been reduced to pole, since this mathematical operation assumes that the survey was flown on a flat, horizontal surface and that remanent magnetization is directed parallel to the Earth's magnetic field. Neither of these assumptions are strictly valid for our magnetic survey, although. Moreover, reduction to the pole would have little effect on these magnetic anomalies since both the total magnetization and ambient field vectors are nearly vertical at this high latitude. TMA gridded data are shown in Figure 2a.

3.1.2. Digital Enhancement & Automatic Lineament Detection

Digital Enhancement techniques are usually employed in potential field geophysics to recognize geological and structural features such as faults, lithological contacts and other structures causing a sharp variation of a physical property (in our case magnetization). Hence, in a continent like Antarctica where rock outcrops and main tectonic structures are almost completely covered by the ice sheet, digital enhancement techniques play a crucial role in the reconstruction of the expected geological and structural framework of complex areas like the MVF. For this reason, we have (a) upward-continued our TMA data to understand the nature of the sources of the magnetic anomalies in the dataset and (b) implemented an image analysis algorithm based on the Hough transform (Duda & Hart, 1972; Hart, 2009; O'gorman & Clowes, 1976) to be applied to the tilt derivative (TDR; Fairhead, 2016; Miller & Singh, 1994; Verduzco et al., 2004) of our TMA data, to unveil with unprecedented detail the main structural features affecting the subglacial MVF.

Regarding the first target, the TMA dataset was upward-continued to 8 km height in order to better isolate and describe the long wavelength magnetic signatures in the data, reflecting the main structures expected in the deeper part of the volcanic complex. Since our TMA data were acquired in a draped mode, to correctly perform their upward continuation we have moved data observations to a flat 8 km height horizontal surface using the Compu-drape package provided in the Geosoft 8.5 Standard Edition suite (https://www.seequent.com/products-solutions/geosoft-oasis-montaj/). The upward-continued data gridded are shown in Figure 2b. At a first glance, the original TMA grid shown in Figure 2a reveals two similar magnetic signatures beneath MM and WR, characterized by wide NW-SE to N-S trending long wavelength pervasive negative anomalies superimposed by apparent short-wavelength positive ones forming radial patterns. Looking at the upward-continued data, the radial pattern completely disappears, leaving very mild positive anomalies on MM and WR surrounded by dominating negative signatures.

For the second purpose, we calculated the TDR of our gridded TMA, being this type of data enhancement especially suitable to detect the edges of magnetic sources with geological significance (e.g., Salem et al., 2007), such as fault-related dikes, cones alignments, lava flows, and so on. Differently from other digital enhancement techniques, the TDR is independent from the magnetization direction (Fairhead, 2016), making it particularly useful in volcanic contexts where usually the remanent magnetization dominates upon the induced one. The TDR map is shown in Figure 3a. To detect the magnetic lineaments, we have first applied the phase congruency operator (Kovesi, 1999, 2003) to the TDR, tracing the local positive picks. The reason of this choice is that we

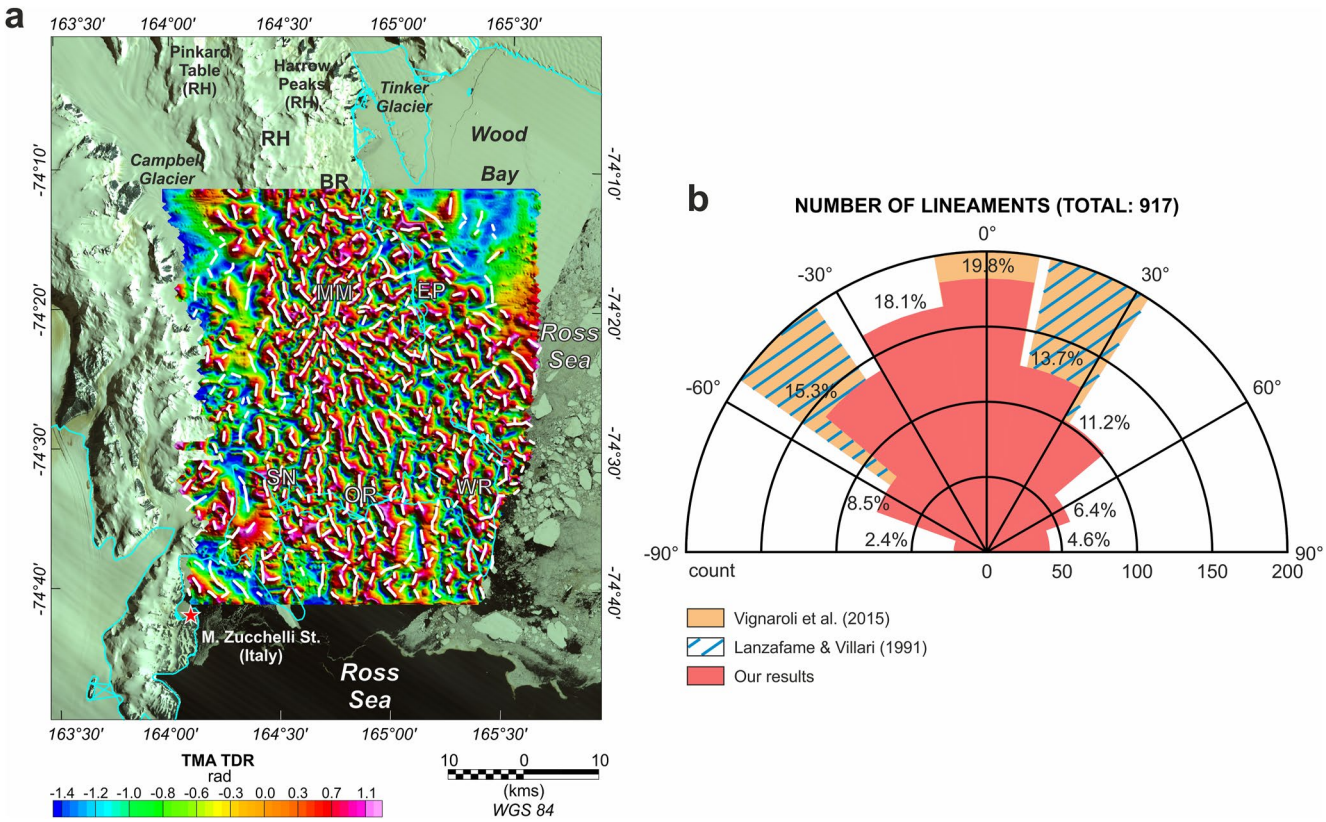

Figure 3. (a) Lineaments detected by the proposed algorithm for automatic lineament detection through the Hough Transform (total amount of lineaments: 917), superimposed on the TDR of our TMA dataset. For abbreviations and symbols see caption of Figure 1. (b) Rose diagram of the percentual frequencies of the detected magnetic lineaments trends. In the background, trends resulting from field surveys of Lanzafame and Villari (1991) and Vignaroli et al. (2015). The N-S trend is the most frequent in the entire MVF.

are interested to detect the traces between the edges bordering fault-related dikes, cones alignments, lava flows, that is, narrow and elongated geological features. The further advantage is that the total number of lineaments detected is approximately halved, simplifying interpretation of results. Then, we have transformed the phase into a black and white image and applied a skeleton algorithm (Lee et al., 1994) to reduce the binary image to 1-pixel wide curved lines without changing the essential structure. At the end, we have applied the Hough Transform to automatically detect and statistically analyze the lineaments in the image. The minimum length detection threshold was placed equal to the magnetic data spacing (500 m). All the structures detected are shown in Figure 3a. To better visualize the structural information achieved, a rose diagram representing the frequency of all the inferred features in respect to their angular orientation is shown in Figure 3b and compared with the trends resulting from Lanzafame and Villari (1991) and Vignaroli et al. (2015) (Figure 1b).

Our results, discussed more in detail in the next sub-Section 3.3, reveal a spread of structural features, mainly distributed between NW-SE and NNE-SSW. These results are in good agreement with published data of tectonic structures measured directly in the field. Such measurements were obtained from data collected from a few scattered outcrops, while our results have a broader coverage being derived from the HRAM data. The minor E-W trending set detected is likely devoid of geological significance, being mainly the result of residual leveling errors not removed during the TMA data processing. Overall, the method proposed in this paper has been capable of also detecting minor trends (see the rose diagram in Figure 3b), proving to be an excellent support for structural studies in remote areas.

3.2. Rock Magnetism

Magnetic properties on rock samples represent fundamental constraints to magnetic inverse modeling, particularly in volcanic environments. The only susceptibility and remanent magnetization measurements on rock

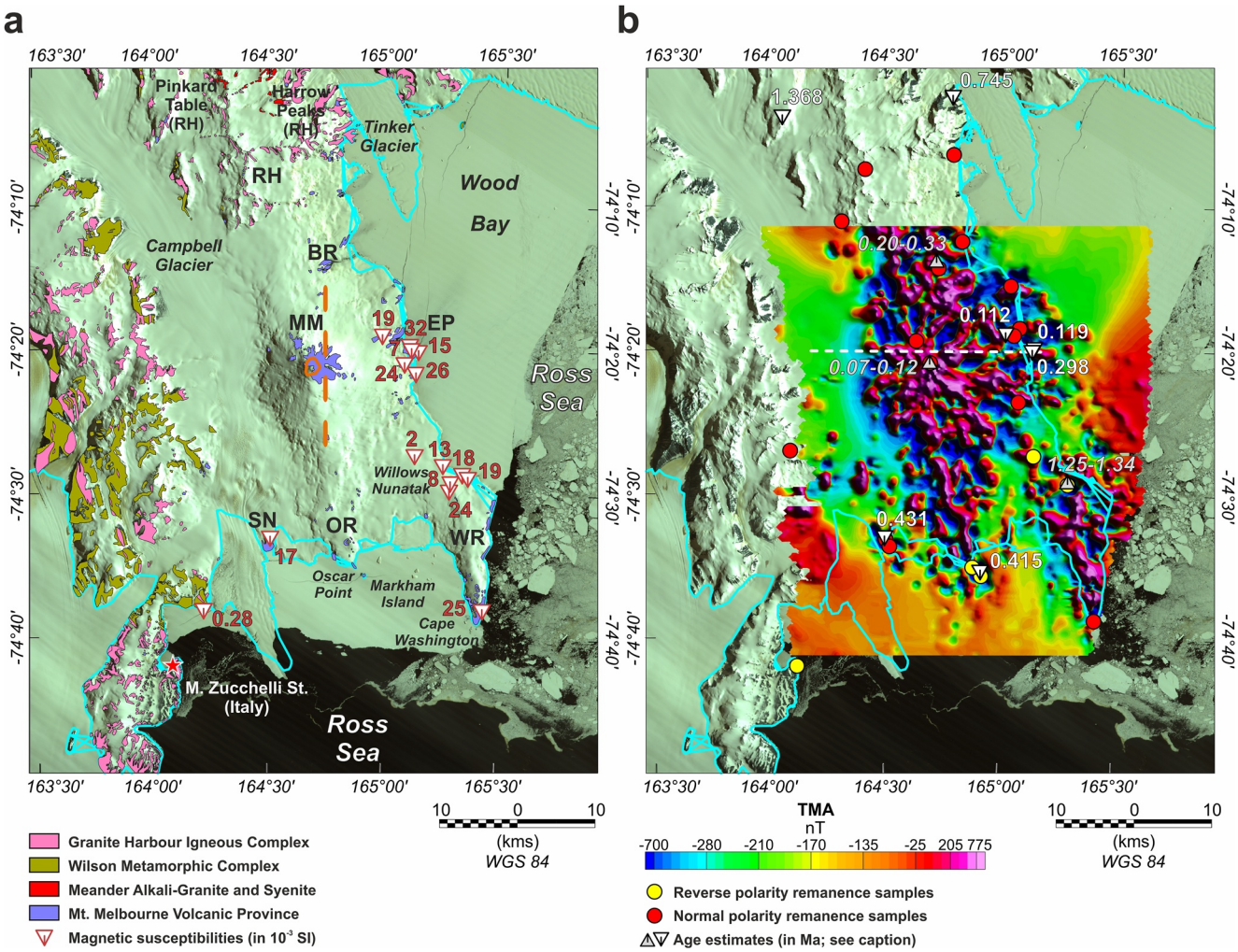

Figure 4. (a) Location and values of the new magnetic susceptibility measures (red numbers and inverted triangles) collected around the MVF (listed in Table S1 in Supporting Information S1) and geology of the study area on Landsat image. Notice the very low value in magnetic susceptibility shown by the only sample collected on the Granite Harbor Igneous Complex compared to all the other ones. In addition, the crater area affected by hydrothermal activity and the trace of a cliff with altered lithologies exposed, discussed in Giordano et al. (2012), are shown in orange. See caption of Figure 1 for abbreviations and other symbols. (b) Locations and values of the most recent age estimates together with magnetic remanence polarity data from literature (base map is Landsat image of the MVF with superimposed the TMA grid). Inverted white triangles and white numbers are the age estimates from Giordano et al. (2012), light gray triangles and numbers in italics are ages from Lee et al. (2015). Other available ages (discussed throughout this manuscript) are not shown due to either missing or imprecise location of the samples (all ages are listed in Table S2 in Supporting Information S1). Magnetic remanence sample data are from Manzoni and Miletto (1988) and Lanza et al. (1991). Moreover, in dashed white is shown the E-W profile along which has been achieved the 2D forward magnetic model illustrated in Figure 7.

samples collected in the MVF were carried out during the 1985/1986 and 2002/2003 Italian Antarctic expeditions to Victoria Land (Bozzo et al., 1987; Lanza et al., 1991; Manzoni & Miletto, 1988; Pasquale et al., 2009). In addition, other unpublished magnetic susceptibility data collected in the field during the 2002/2003 Italian Antarctic expedition are presented in this work. These data have been measured by means of a portable kappa-meter Geofyzika KT5 with a resolution of 10^{-5} SI units, collecting for each site up to 12 measurements to be able to make a statistical evaluation of the quality of the data. Locations and magnetic susceptibility data from the new samples analyzed are shown in Figure 4a and listed in Table S1 in Supporting Information S1. In the same table, are listed also all previous magnetic property data available for the MVF.

The large variability in magnetic susceptibility shown by rock samples, even belonging to the same outcrops (Table S1 in Supporting Information S1), reflects the petrographic and textural heterogeneity of rocks observed in this volcanic area (Wörner et al., 1989) and, consequently, the variable content and type of ferromagnetic minerals in magmatic products (Clark, 1997; Hinze et al., 2013). A similar argument applies to the magnetic

remanence, reaching in some places very high values (>20 A/m, see Table S1 in Supporting Information S1). Furthermore, the widespread prevalence of very high Koenigsberger ratios (i.e., the ratio of Remanent magnetization and Induced magnetization modules) suggests the magnetic susceptibility of rocks could be neglected during modeling of TMA data (Manzoni & Miletto, 1988).

For what concerns the inclination of magnetic remanence, assuming no continental-scale tectonic displacement/rotation occurred in this part of Antarctica during the Quaternary period, it is representative of the polarity of the Earth magnetic field recorded by rocks after their cooling. In detail, samples with both normal (i.e., negative remanence inclination) and reverse (i.e., positive remanence inclination) polarization were found in MVF, the reverse ones located on OR area (also southward to Markham Island), north of WR and on the south-eastern slope of the MM (Figure 4b). Since the times of the magnetic polarity reversal are well known, these remanence data are fundamental to (a) document certainly that volcanic activity started before the current Brunhes magnetic epoch (>0.78 Ma, chron C1n following the notation proposed by Cande & Kent, 1992, 1995) and (b) correctly assess the anomaly sources in our HRAM dataset. Hence, coupling available geochronological data from rock samples collected around the field we can finally have a look at the inner buried MVF and obtain important hints to reconstructing the timing of the volcanic activity, as we discuss afterward.

3.3. HRAM and Rock Magnetism Interpretation Combined With Available Geochronological Data

Our analysis and enhancement of TMA data supplied new detailed information about (a) the sub-ice structural lineaments and (b) the buried volcanic framework characterizing the MVF.

Regarding point (a), subglacial sets of features trending mainly between NW-SE and NNE-SSW have been detected through automatic lineament detection, with the N-S trend more pervasively distributed and matching the topographic orientation of both the WR and the MM (Figure 3). Our observations can be compared with structural data available in literature and derived from either direct field investigations or aerial image analysis (e.g., Giordano et al., 2012; Lanzafame & Villari, 1991; Vignaroli et al., 2015, Figures 1b–3). Our lineaments fit the orientation of the main tectonic structures and fault-related dikes, subaerial alignments of volcanic scoria cones and lava flows described for the MVF area, striking approximately N-S at OR and WR and NE-SW at EP (Wörner & Viereck, 1989). The N-S to NW-SE trending lineaments likely can be associated with a strike-slip deformation pattern (e.g., Läufer et al., 2011; Salvini et al., 1997; Storti et al., 2008) and seem to link the MM area to RH northward and OR southward, suggesting a common structural control on the volcanic activity generating these sub-suites. The NNE-SSW trend appears to connect MM to the EP sub-suites, inferred the result of a Quaternary change in the deformation regime that involved the activation of major extensional fault zones along the modern coastline (Vignaroli et al., 2015). Moreover, both MM and WR lineaments follow the already described radial pattern in the TMA grid. Such a pattern could be associated with both (a) radial lava flow events steered by the topographic gradient and (b) swarms of radial dikes of volcano-tectonic origin. Evidence of radial lava flows is suggested by field observations on the crater area of MM (Wörner & Viereck, 1989), whereas radial swarms of dikes could be emplaced in the fissures of the volcanic edifices generated by a local stress field change related to the rise of magma inside the volcano (e.g., Geshi, 2008 and references therein).

As regards the buried volcanic framework characterizing the MVF (point b), two similar magnetic signatures beneath MM and WR have been recognized, characterized by strong and distinct positive and negative anomalies.

The positive anomalies, commonly showing a radial pattern on MM and WR as just indicated by results from automatic lineament detection (Figure 2a–3a), are related to short-wavelength signal components due to sources characterized by different magnetic properties in respect to surrounding volcanics, as suggested by upward-continued TMA data (Figure 2b). These magnetic sources may be associated with volcanic activity, in the form of swarms of feeder dikes and related lava flows, occurred during periods of magnetic normal polarity. These could be either the current Brunhes epoch (C1n < 0.78 Ma) or the Jaramillo (C1r.1n) and Olduvai (C2n) chrons (1.07–0.99 Ma and 1.95–1.77 Ma, respectively), short intervals in the reverse magnetic polarity Matuyama epoch (2.58–0.78 Ma). The Brunhes hypothesis is in better agreement with the consistent observation of geochronological data younger than ~0.50 Ma and normal polarity from most of the rocks of the MM slopes and the peripheral southwestern SN and eastern EP centers, the last considered one of the youngest volcanic sub-suites of the MVF (see Figure 4b; Armstrong, 1978; Kreuzer, 1988 - unpubl. report; Armienti et al., 1991; Giordano et al., 2012; Lee et al., 2015; Müller et al., 1991). In the summit of MM, positive magnetic anomalies,

field evidence and historical observations on ice thickness indicate volcanic activity occurred until recent times (Adamson & Cavaney, 1967; Del Carlo et al., 2022; Keys et al., 1983; Lee et al., 2019; Lyon, 1986; Nathan & Schulte, 1968); the latter eruptions deposited tephra layers thick about 5 m in the eastern crater rim (Wörner & Viereck, 1989). For a comprehensive overview of all age estimates and magnetic remanence inclination data available for each volcanic sub-suite, refer to Table S2 in Supporting Information S1.

As far as the other peripheral centers to the north, at BR (Figure 4a) ages are available for both the coastal and inland sectors, showing a younging of rocks moving inland. Ages from the inland area are 0.72 ± 0.10 and 0.19 to 0.33 Ma (Armstrong, 1978; Lee et al., 2015), whereas those in the coast to the north are 2.59 ± 0.11 and 2.96 ± 0.20 Ma (Armienti et al., 1991). All these age estimates are placed in periods of normal polarity, the oldest in the Gauss epoch and the youngest in the current Brunhes, in agreement with remanence negative inclinations from rock samples collected in this area.

For the northernmost RH (Figures 4a) Armienti et al. (1991) reported age estimates of about 12.50 Ma, much older than all the others available for the MVF, whereas Giordano et al. (2012) indicated younger ages of 0.745 ± 0.066 and 1.368 ± 0.090 Ma (Figure 4b). If we take into account only the more recent ages proposed by Giordano et al. (2012), owing to the limitations of the K-Ar method used by Armienti et al. (1991) for dating, the formation of the RH volcanic centers likely started in the Matuyama epoch and continued in the current Brunhes epoch, as suggested also by normally-polarized remanence samples from that area.

Regarding the southeastern WR area (Figure 4a), ages ranging from 2.70 to 1.67 Ma (Kreuzer, 1988 – unpubl. report) coupled with normally-polarized remanence samples (see Figure 4b) suggest the positive radial pattern in this area could be the response of lava flows deposited either during the Olduvai chron or, as pointed out by Lanza et al. (1991), at the end of the Gauss epoch, being the oldest age estimates placed before the Gauss – Matuyama polarity reversal (2.58 Ma). As a support for both the hypotheses, the remanence samples, located where positive magnetic anomalies occur, are surrounded by negative ones, most likely related to magmatic activity occurred in the Matuyama epoch; in fact, the preceding reverse polarity Gilbert epoch would be too older (5.89–3.58 Ma) in respect to the ages available on WR (Armstrong, 1978; Kreuzer, 1988-unpubl. report).

The negative magnetic signatures, which dominate the enhanced TMA data (Figure 2b), could be related to a combination of different phenomena, that are (a) strong demagnetization owing to intensive hydrothermal alteration, (b) topographic effects, (c) lava flows with highly variable content in magnetic minerals (i.e., strong contrasts in magnetic susceptibility/remanence), and (d) thick volcanic strata with reverse magnetization.

Regarding the demagnetization hypothesis (point a), various authors described the presence of weak and scarce geothermal surface manifestations around MM such as fumarolic activity, steaming grounds and ice hummocks focused on the north rim and slope of two craters in the southern side of the crater (Cremisini et al., 1991; Gambino et al., 2021; Lyon & Giggenbach, 1974; Nathan & Schulte, 1967; Figure 4a). In addition, hydrothermal alteration is pointed out by Giordano et al. (2012) along a sub-vertical cliff about 50–100 m high running N-S along the entire eastern flank of MM (Figure 4a). The effect of a hydrothermal circulation in a volcanic environment is the loss of magnetization from magnetic minerals contained abundantly on rocks, resulting in a smooth attenuation of magnetic anomalies following the location of geothermal surface manifestations (e.g., Bouligand et al., 2014; Finn et al., 2007; Finn et al., 2022; Finn & Morgan, 2002). This phenomenon has not been observed in the MVF, suggesting the absence of a spread and consistent deep hydrothermal circulation (Figure 4b). As a validation of this evidence, Lyon and Giggenbach (1974), Cremisini et al. (1991), and Gambino et al. (2021) suggested that the hydrothermal manifestations of the MVF, showing very low pressure and intermittent activity in some locations, could derive from melted buried ice. Hence, hydrothermal manifestations and alterations would be the result of localized and superficial hydrothermal activity not affecting in depth the magnetic properties of rocks in the MM. In light of these considerations, the first hypothesis seems less probable.

As far as hypotheses (b), 3D forward modeling has been performed to test the topographic effects by means of the Parker's algorithm (Parker, 1972), as implemented in the software package GMSYS-3D (Geosoft 8.5 Standard Edition). Differently from the original Parker's algorithm, such implementation allows the computation of the magnetic response on observation points arranged in a draped fashion, as is the case with our survey (i.e., observation points are maintained at their original height and resolution as described in sub-Section 3.1.1). The model geometry is 36.5 × 53.1 km wide in the East and North direction, respectively, designed to include the main volcanic sub-suites only. The approach chosen requires a model geometry defined by surfaces, infinitely

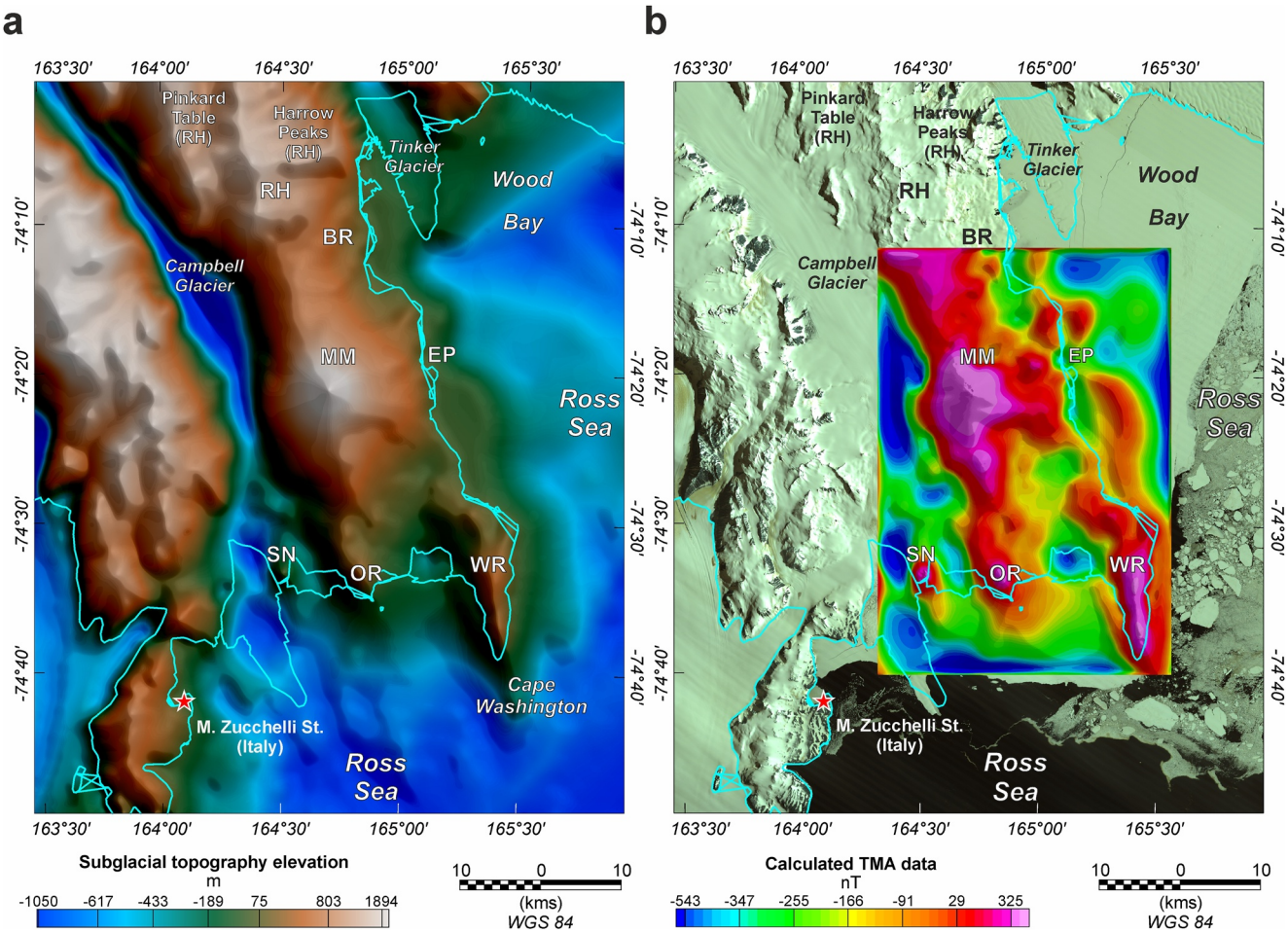

Figure 5. (a) Subglacial topography from BedMachine v.2 data (Morlighem et al., 2020). (b) TMA response of the topography from the 3D Parker's forward model described in sub-Section 3.3. For abbreviations and symbols see caption of Figure 1.

elongated outside the model, which separate layers with fixed magnetic properties. Since our aim is to calculate the magnetic response of the topography, surfaces defined are the top and the bottom of the model. The top is represented by the subglacial topographic surface defined by BedMachine v.2 data with a resolution of 500 m (Morlighem et al., 2020, Figure 5a), re-gridded at 100 m in accordance with our model resolution. The bottom surface is placed at the constant elevation of −2,500 m; a different elevation would not have affected the results since the magnetic response of a flat, uniformly magnetized, and infinitely elongated layer is zero (Blakely, 1996). The magnetized layer enclosed between the top and the bottom surfaces is characterized by induced magnetization only, with module, inclination and declination of 5 A/m, −83.1° and 133.2°, respectively. Such a magnetization module value has been chosen so that computed positive magnetic anomalies match as much as possible with those in our TMA dataset, whereas the inclination and declination agree with those of the Earth's magnetic field in the study area when the survey was flown. The resulting magnetic contribution of the topography is shown in Figure 5b. As it can be seen, negative anomalies in our TMA dataset are too intense to be explained by terrain effects due, for example, to subglacial valleys. The only exception relates to the negative anomaly around the western flank of the MM caused by the southern part of the Campbell Glacier valley (Figure 5), whose bed has recently been better characterized through a helicopter-borne ice penetrating radar survey (Lee et al., 2021). Elsewhere, we cannot exclude that the deposition of lava flows could have been influenced by valleys excavated by erosion along radial-shaped volcano-tectonic fractures during periods of volcanic quiescence, generating low-amplitude anomalies elongated along the valleys themselves.

Regarding point (c), a strong contrast in magnetic mineral content among lava flows and surrounding volcanics is not enough to explain the alternation of strong negative and positive anomalies in our TMA dataset. The

proof come from the summit area of MM, characterized by strong positive magnetic anomalies despite available samples show low values in magnetic remanence module. This suggests local less magnetized volcanics and lava flows do not significantly affect the TMA signal, since it is dominated by surrounding more magnetized rocks.

In light of above, the best explanation that fits for such strong negative anomalies in our TMA dataset is the occurrence of reversely-polarized rocks, as commonly found in volcanic environments (e.g., Blanco-Montenegro et al., 2018; Dumont et al., 2021). An example come from the Piton des Neiges volcano (Réunion Island), where paleo-valleys excavated in reversely-polarized volcanics and filled by normally-polarized lava flows have been clearly recognized by performing a HRAM survey (Dumont et al., 2021; Martelet et al., 2014). In this volcano, the magnetic signature of the filled paleo-valleys forms a positive radial pattern surrounded by strong negative anomalies, similarly to that recognized in our TMA dataset.

Moreover, in the MVF reversely-polarized remanence has been found in samples from some outcrops in northern WR, Willows Nunatak (at the south-eastern slope of MM) and in OR area (including Markham Island), indicating volcanic activity during the Matuyama epoch (Figure 4b). This evidence is supported by geochronological data older than the last magnetic polarity reversal (i.e., 0.78 Ma) for WR, Willows Nunatak and SN (Figure 4b; Table S2 in Supporting Information S1).

Regarding Willows Nunatak/north of WR, close to the reversely-polarized remanence samples, five ages of 2.40 ± 0.10, 1.25 ± 0.09, 1.34 ± 0.07, 1.31 ± 0.09, and 1.32 ± 0.07 Ma were estimated (Armstrong, 1978; Lee et al., 2015). Since Willows Nunatak is located at the basal slope of MM, the just described age estimates are a strong clue pointing to a beginning for the magmatic activity that built-up the MM edifice at least during the Matuyama epoch, namely much earlier than previously thought. This hypothesis is strengthened by trachytic xenoliths found in the Mt. Melbourne pyroclastics, interpreted possibly as old as 2.5 Ma (Wörner & Viereck, 1989), placed in time at the beginning of the reverse polarity Matuyama epoch.

For the OR area, the geochronological data available indicates discordant ages of 0.71 ± 0.18 Ma and 0.415 ± 0.024 Ma (Armienti et al., 1991; Giordano et al., 2012). The first age straddles the transition of the Matuyama and Brunhes epochs, while the second is in the current Brunhes epoch and appears in disagreement with reversely-polarized remanence data. However, the magnetic signal upon Markham Island shows a local moderate increase in TMA in respect to surrounding strong negative values, suggesting a possible intrusion of a small younger normally-polarized volcanic body. Hence, all evidence suggests this peripheral volcanic center could have formed just before the last magnetic polarity reversal, continuing to develop until more recent ages.

Regarding SN, ages of 1.56–1.77 Ma are available for a basal mugearitic lava flow (Kreuzer, 1988-unpubl. report; Müller et al., 1991). These ages refer to samples collected above an erosional unconformity separating the basal mugearitic lava flows from overlying younger alkali-basalts interbedded with subaerial tephra (Wörner & Viereck, 1987, 1989), for which two age estimates of 0.48 ± 0.24 and 0.43 ± 0.08 Ma are available (Armienti et al., 1991; Giordano et al., 2012). For the sake of completeness, another age of 0.07 ± 0.05 Ma was documented for an upper alkali basalt flow (Kreuzer, 1988-unpubl. report) but would be unlikely and possibly affected by some analytical error (Giordano et al., 2012). Interesting information comes from a normally-polarized remanence sample collected in the basal SN, whose inclination is lower (in absolute value) compared with another near normally-polarized sample, relative to the upper alkali-basalts (Figure 4b, see Tables S1–S2 in Supporting Information S1). As a possible explanation for the sample showing lower remanence inclination, Lanza et al. (1991) suggested either (a) outcrop displacement or (b) lava flow emplaced during a magnetic polarity transition. Following the last hypothesis, the younger portion of the basal mugearitic lava flows could be deposited at the transition among the Matuyama epoch and either the Jaramillo chron or the Brunhes epoch, being the overlying alkali-basalts spread out certainly in the Brunhes epoch as suggested by geochronological data. Moreover, these remanence samples are located at the boundary between a strong positive and negative magnetic anomaly, documenting likely a contact between normal and reverse polarity volcanic products. Therefore, also in this area there is strong evidence of a magmatic activity started prior to the last magnetic polarity reversal.

All the evidence described above is quite strong, that is all the normal remanence samples are always located upon or near areas of magnetic positive anomaly and vice versa all the reverse remanence samples are placed upon or near magnetic negative anomalies (see Figure 4b).

In addition, reversely-polarized remanence samples give us other important structural information that would have affected first lava depositions. In fact, all these samples show ENE-WSW oriented magnetic lineations

(Lanza et al., 1991), suggesting first lava flows driven by NW-SE to N-S fissures on the crystalline basement of the Ross Orogen Wilson Terrane, in the assumption of a low topographic gradient. Magnetic lineations, defined by the directions of maximum susceptibility, are indeed known to commonly reflect the direction of the lava flows (Hrouda, 1982; Tarling & Hrouda, 1993).

In summary, our findings suggest the inner structure of the MVF could be approximated by a NW-SE to N-S elongated thick reversely-polarized volcanic unit built-up during the Matuyama epoch, overlying the Ross Orogen Wilson Terrane, intruded by swarms of fault-related dikes and surmounted locally by lava flows, deposited during normal polarity chrons and forming the present-day main volcanic centers. On MM and WR, normally-polarized lava flows deposition may have been guided by radial paleo-valleys floored by the reversely-polarized basal unit, as supported by the characteristic magnetic pattern seen in our TMA data.

4. Inverse Modeling

All the geophysical evidence discussed above points for the MVF to a general magnetic structure characterized by a basal reversely-polarized volcanic unit, covered locally by an upper normally-polarized one on the main volcanic centers. The magnetic responses of these two units are quite distinct in the TMA signal, since the long-wavelength components are related to the basal reversely-polarized volcanics and the short-wavelength ones to swarms of normally-polarized dikes and related lava flows. Hence, we have applied a two-step procedure to image the inner framework of the MVF.

1. modeling of long-wavelength components using the 3D Parker-Oldenburg's method;
2. modeling of short-wavelength components by an “ad hoc” developed approach.

A step-by-step inversion procedure may be particularly useful in complex geological contexts like the MVF, as it is capable of (a) addressing several independent targets subsequently and (b) keeping more manageable the non-uniqueness arising in such complex scenarios in respect to using a single inversion approach.

In detail, Parker-Oldenburg's method (Oldenburg, 1974; Parker, 1972) is an inverse approach based on the Parker's forward algorithm, considering a set of layers with the top and bottom boundaries defined by arbitrary surfaces, hence it is particularly suitable to define the geometry of the basal reversely-polarized volcanic unit. The upper unit, between the subglacial topography and the top of the basal reversely-polarized unit, is instead modeled using vertical 3D prisms with variable intensity of magnetization (Bhattacharyya, 1964), suitable to image the dike and lava flow distribution that affects in particular MM and WR areas. For this second step, the dataset to invert is the original TMA from which the contribution of the basal reversely-polarized unit, obtained at point i), is subtracted. The two-step approach is presented in detail in the next sub-Sections 4.1 and 4.2.

4.1. Modeling of Long-Wavelength Signal Components

The methodology used to define the main volcanic units characterizing the MVF is based on Parker-Oldenburg's approach (Oldenburg, 1974; Parker, 1972) as implemented in the software package GMSYS-3D (Geosoft 8.5 Standard Edition); the Parker forward algorithm has been already described in sub-Section 3.3. The model geometry is, again, 36.5 × 53.1 km wide in the East and North direction, respectively, being designed to not include northward the smaller volcanic centers of RH, possibly characterized by different geological settings. In fact, these scattered volcanics are inferred to be resting directly on the Ross Orogen Wilson Terrane (Figure 1b). Observation points are maintained at their original height and resolution as described in sub-Section 3.1.1. The top of the model is represented by the subglacial topographic surface defined by *BedMachine v.2* data (Morlighem et al., 2020), whereas the bottom surface is placed at the constant elevation of −2,500 m for the same reason explained in sub-Section 3.3 about the 3D forward calculation test. According to the hypothesis proposed above about the inner structure of the MVF, the geophysical setup of the model consists of two overlapping layers characterized by opposite magnetic polarity, the deeper reverse and the shallower normal. Since the target of the Parker-Oldenburg's inversion method is represented by the geometry of the surface separating the two layers, their magnetization properties are maintained constant during the inversion. The starting elevation of this surface was placed at −1,000 m, below the most depressed topographical point of the MVF. For physical consistency, an underneath layer representing the crystalline basement of the Ross Orogen Wilson Terrane is not entered. The reason of this choice is due to (a) the lack of knowledge about the geometry of the basement and (b) its negligible

magnetic response compared to the overlying strong-remanence volcanic flows, as suggested by susceptibility data available in the literature about the Ross Orogen Wilson Terrane (Bozzo et al., 1991; Talarico et al., 2003; see Figure 4a). As a constraint for the inversion results, we have used the magnetic remanence data from Manzoni and Miletto (1988) and Lanza et al. (1991) to define averaged magnetic properties for the two modeled layers (see Table S1 in Supporting Information S1). Magnetic susceptibility has not been considered owing to the high Koenigsberger ratio shown by rock samples from the MVF (Table S1 in Supporting Information S1), suggesting dominant remanence as already explained (see Manzoni & Miletto, 1988). The samples MB4, MB11, MB16, MB21, MB27, MB29 have not been considered for the calculation of the averaged magnetic properties due to their low-angle inclination values, explainable likely by limited gravitational or tectonic displacements (Lanza et al., 1991). Sample MB29 has been discarded as a precaution, because it could also document a magnetic polarity transition. In summary, the deeper layer is set with average values of magnetic remanence module, inclination and declination of 5.63 A/m, 78.02°, and 161°, whereas the shallower 8.08 A/m, −75.35° and 143.3°, respectively. The Earth's Magnetic Field module, inclination and declination values were 64,413.5 nT, −83.1° and 133.2° when the survey was flown.

The results from the inversion are shown in Figures 6a and 6b, in the form of (a) geometry of the inverted contrast surface and (b) thickness of the shallower volcanic unit with inferred normal polarity. A misfit grid among our TMA dataset and the calculated response of the model from inversion is shown in Figure S3 in Supporting Information S1. The inverted surface (point a), whose shape has been achieved after 21 iterations, shows pronounced corrugation and seems to image vertical features cutting the underneath reversely-polarized magnetic lava flows (Figure 6a). Similar features, geologically explainable as vertical swarms of feeder dikes, are quite evident in MM area likely as a consequence of the volcanic activity that occurred in the current Brunhes epoch, significantly affecting the basal reversely-polarized unit. For what concerns point (b), it has been achieved as a difference among the subglacial topography grid with the inverted magnetic contrast surface (Figure 6b). Results suggest that the areas in MVF characterized by non-zero thickness of normal polarity volcanic rocks can be found at MM, BR, WR, SN, OR, and in part at EP, namely in the main volcanic centers of the MVF. Elsewhere, reversely-polarized volcanics are expected to outcrop on the subglacial topography, in good agreement with the locations of reversely-polarized magnetic samples (Figure 6b).

However, looking at the calculated TMA grid from the Parker-Oldenburg's model, it can be noticed that the positive anomalies are not well matched in shape and values, since they lack the radial pattern described in the observed TMA data particularly in the MM and WR areas. On the contrary, the background negative anomaly in the observed and calculated TMA data (see Figure S3 in Supporting Information S1) appears very similar, particularly in shape. Hence, the hypothesis of a basal reversely-polarized volcanic unit with homogenous magnetic properties explains well the long-wavelength components of the TMA signal. The non-fitted short-wavelength components of the TMA data, representing the positive anomalies, point to an upper unit that is not as homogenous as the basal one, in which the magnetization is expected to vary laterally also in polarity. The reason for this could be found in a thicker reversely-polarized basal volcanic unit intruded by swarms of normally-polarized feeder dikes and surmounted by related lava flows particularly on the MM edifice and WR.

As discussed in the introduction of Section 4, this lateral variation in magnetization, expected for the shallower parts of the main volcanic centers, is the target of an “ad hoc” developed approach. The detailed settings and results of this methodology are presented in the next sub-Section.

4.2. Modeling of Short-Wavelength Signal Components

Our purpose here is to assess the variability in magnetization expected in the upper volcanic unit of the main sub-suites of the MVF to address the sources of the positive anomalies in the TMA dataset, including the characteristic radial pattern. To accomplish this, we consider the same model geometry used for the Parker-Oldenburg's model and a discretization of the study area involving vertical prisms, whose top is defined by the *BedMachine v.2* subglacial topography and the bottom confined by the contrast surface achieved through the previous Parker-Oldenburg's inversion. Vertical prisms, each with horizontal dimensions of 250 × 250 m, are defined where the subglacial topography does not match the contrast surface (i.e., no zero-thickness of the upper volcanic unit in Parker-Oldenburg's model in the previous sub-Section). Hence, the total number of prisms considered is 11,219 out of a total of 31,311 possible locations. Observation points are maintained again at their original height and resolution as described in sub-Section 3.1.1. The model parameters are only the intensity of magnetization

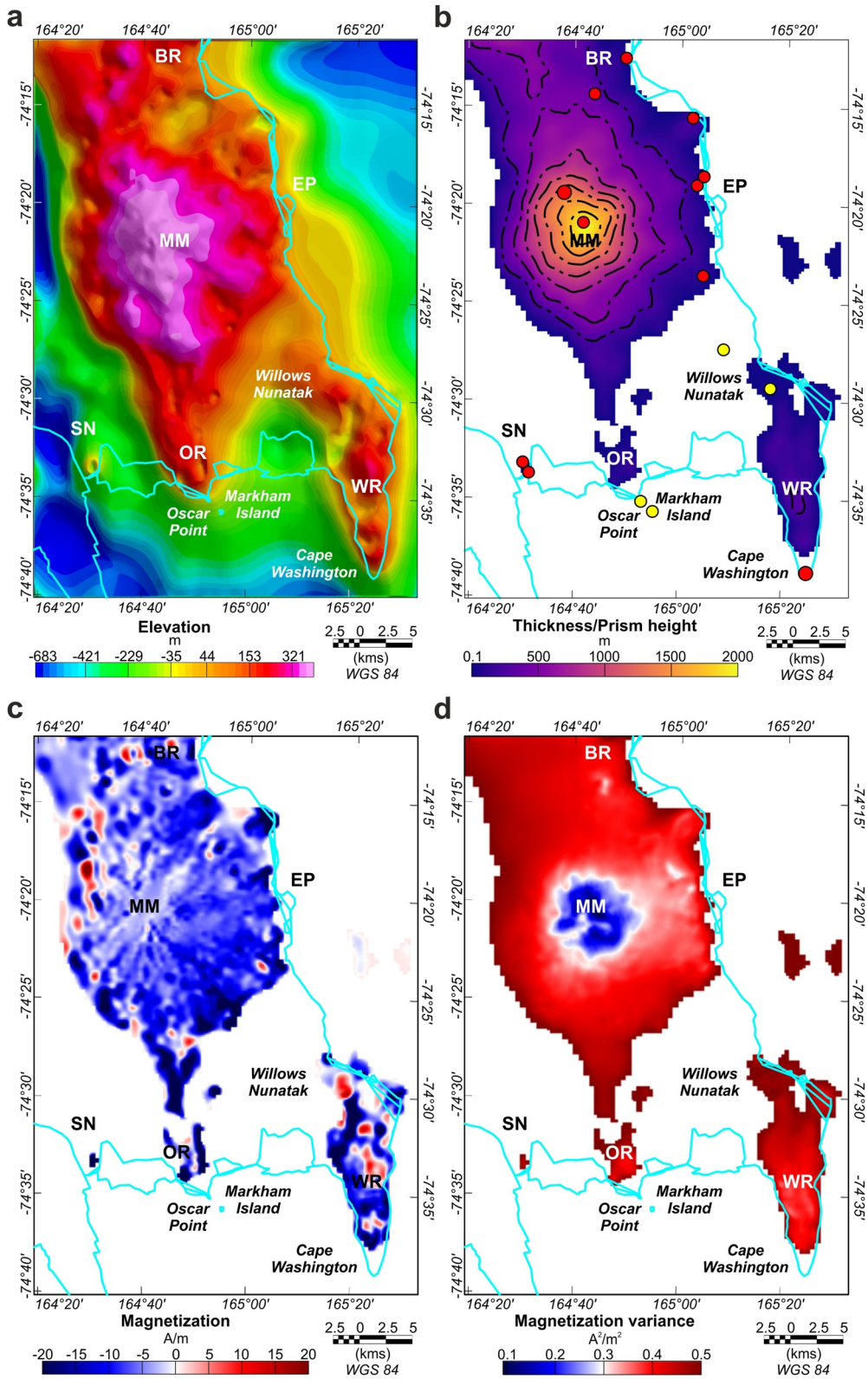

Figure 6.

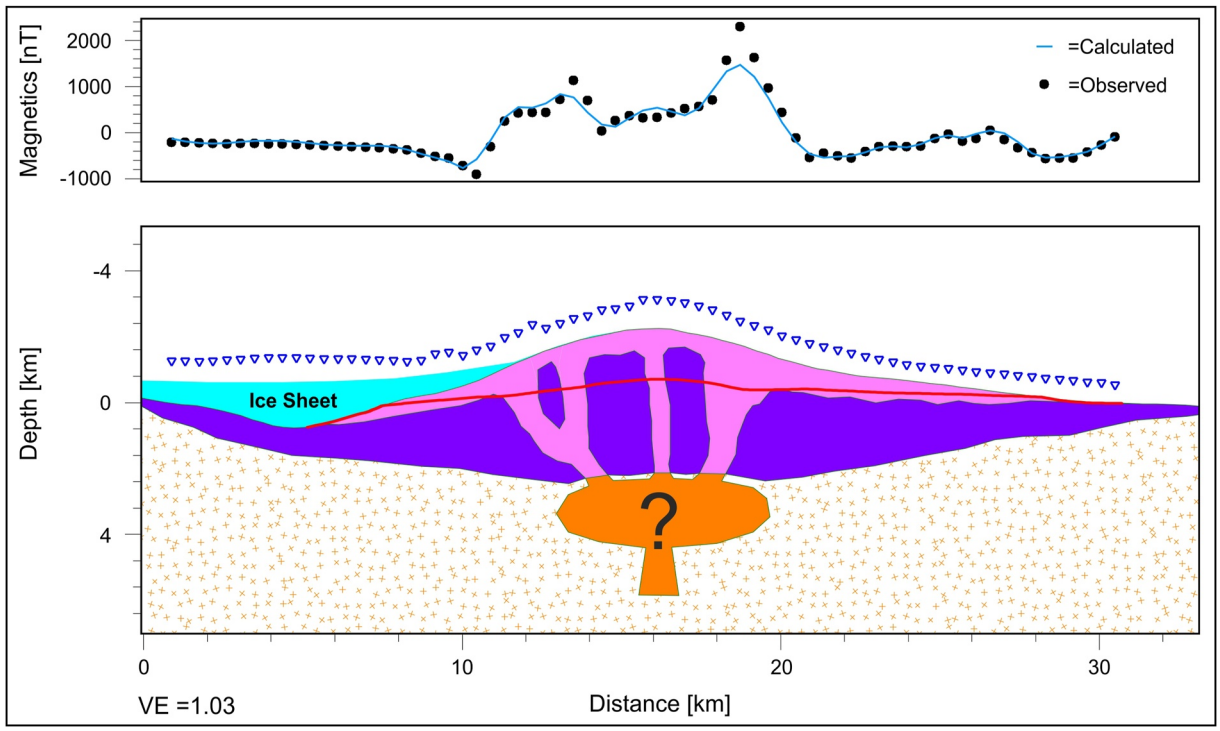

Figure 7. 2D forward model showing the inner structure below MM along the E-W profile displayed in Figure 4b (vertical exaggeration equal to 1.03). A total number of 69 observation points are indicated as inverted blue triangles in the second panel, whereas the respective measured data and the calculated response of the model are shown in the first panel. In pink are modeled normally-polarized lava flows and fault-related dikes, whereas in purple reversely-polarized volcanics. The magnetic properties associated to them are only magnetic remanence, with module, inclination and declination of 8.08 A/m, −75.35°, 143.3° and 5.63 A/m, 78.02°, 161°, respectively (same values used for the 3D Parker-Oldenburg's inversion). Below is the Ross Orogen Wilson Terrane, to which is associated only magnetic susceptibility equal to $0.28 \cdot 10^{-3}$ SI (see Figure 4a). In orange is qualitatively indicated a magma chamber, whose actual existence, position and extension are unknown. For a comparison, the trace of the contrast layer among inferred normally- and reversely-polarized volcanics obtained through the Parker-Oldenburg's inversion method is placed on the model. It can be noticed that this contrast surface matches the respective in the 2D forward model particularly toward the external part of MM, where the approximation of two overlapping strata with opposite magnetic properties works well. Conversely, this approximation does not work anymore for the central part of the MM affected by the intrusion of normally-polarized feeder dikes, rather causing a lateral variability in magnetization properties and polarities.

of each prism, with inclination and declination fixed and equal to that of the inducing Earth's Magnetic Field when the survey was flown (−83.1° and 133.2°, respectively). This simplification is possible because at the time of the survey the inducing Earth's magnetic field was almost parallel and anti-parallel to the magnetization vectors obtained from the average magnetic properties of the inferred normally- and reversely-polarized volcanic units presented in sub-Section 4.1 (the main difference lies in the declination values; however, their effect in the magnetic response decreases approaching the Earth's poles). Hence, positive values in the magnetization module will refer to prisms with magnetization vectors having the same direction as that of the current Earth's magnetic field, whereas negative ones will indicate magnetization vectors aligned to the current Earth's magnetic field but pointing in the opposite direction. The advantages of reducing the model parameters in such a way are (a) the decrease of the number of degrees of freedom of the inverse problem and (b) the linear relationship between model parameters and calculated data, considering as forward formulae those from Bhattacharyya (1964). As a result, this approach is easy to handle and setup. Such method shows some similarities with the apparent susceptibility mapping approach (e.g., Grant, 1973; Silva & Hohmann, 1984; Zunino et al., 2009), however, it is

Figure 6. (a) Map showing the elevation of the contrast surface between the basal reversely-polarized unit and the upper volcanic one characterized by highly variable magnetization modules and polarities, resulting from the Parker-Oldenburg's inversion. This surface appears very rough, being the reversely-polarized volcanic bottom likely intruded by swarms of normally-polarized feeder dikes. (b) Map showing the thickness of the upper volcanic unit, obtained as a difference between the subglacial topography and the contrast surface shown in (a). Such unit has been discretized by finitely-elongated vertical prisms, as required by the "ad hoc" inversion approach used in sub-Section 4.2 to characterize the upper volcanic unit inferred on the MVF. Contour lines every 250 m of height. The location of the magnetic remanence polarity samples discussed in sub-Section 3.2 are superimposed on the map (references in Figure 4b). (c) Map showing the magnetization intensity expected for the upper volcanic unit using the "ad hoc" inversion approach. (d) Map of the variance estimated for the magnetization intensity results shown in panel (c). For abbreviations in panels (a)-(d), see caption of Figure 1.

characterized by a different setup (i.e., apparent susceptibility mapping assumes prisms infinitely-elongated in depth) and used in a different geological context.

The dataset to invert was re-sampled at a resolution of 250 m for consistency with the model setup, with a total of 31,311 observation points. This kind of discretization was chosen as a balance between keeping the model resolution high and being able to manage the amount of required computer memory for the matrix representing the forward model. The dataset to invert was obtained by subtracting the total-field magnetic response of the reversely-polarized volcanic unit, whose geometry was figured out through the previous inversion approach, from our TMA dataset. Consequently, the signal obtained should be almost exclusively the response of magnetic sources placed in the upper volcanic unit. The variance associated with each TMA measure is 100 nT^2.

The final model setup is shown in Figure 6b. In order to constrain the solution, we have set prior information about the model parameters in the form of a Gaussian probability density function with mean equal to 1 A/m and variance 0.5 A^2/m^2 (i.e., same mean and variance for each model parameter). This choice reflects our wish to obtain a smooth and geologically plausible map of the lateral variation of magnetization. Following the probabilistic formulation of a linear inverse problem as described in Tarantola (2005), the mean model solution $\widetilde{\boldsymbol{m}}$ (i.e., the intensity of the vectors of magnetization of prisms) is then given by:

$$\widetilde{\boldsymbol{m}} = \left(\boldsymbol{G}^T \boldsymbol{C}_D^{-1} \boldsymbol{G} + \boldsymbol{C}_M^{-1}\right)^{-1} \left(\boldsymbol{G}^T \boldsymbol{C}_D^{-1} \boldsymbol{d}_{obs} + \boldsymbol{C}_M^{-1} \boldsymbol{m}_{prior}\right) \quad (1)$$

where $\boldsymbol{G}$ is the forward matrix, $\boldsymbol{d}_{obs}$ and $\boldsymbol{C}_D$ the observed data and the relative covariance matrix, $\boldsymbol{m}_{prior}$ and $\boldsymbol{C}_M$ the prior model and its covariance matrix (diagonal in our setting). The uncertainty of the mean solution $\widetilde{\boldsymbol{m}}$ is quantified by the posterior covariance $\widetilde{\boldsymbol{C}}_M$, that is:

$$\widetilde{\boldsymbol{C}}_M = \left(\boldsymbol{G}^T \boldsymbol{C}_D^{-1} \boldsymbol{G} + \boldsymbol{C}_M^{-1}\right)^{-1} \quad (2)$$

The results of the inversion are shown in Figures 6c and 6d in the form of maps of intensity of magnetization and its variance, respectively. The low values of variance observed suggest a good reliability of the mean model $\widetilde{\boldsymbol{m}}$. For the sake of interpretation, since the magnetic dipole associated with each prism is nearly aligned to the vertical, this inversion approach is mostly sensitive to anomalous bodies directly below the respective magnetic anomalies. The calculated TMA data, computed as the sum of the total-field anomaly due to the basal reversely-polarized volcanic unit from the 3D Parker-Oldenburg's model and the response from the solution using this inversion approach, is shown in Figure S4 in Supporting Information S1. The calculated data fit very well our short-wavelength TMA dataset. In the areas excluded by this modeling approach, positive peaks visible are likely due to swarms of normally-polarized dikes intruding the reversely-polarized basal unit or directly the low-susceptibility Ross Orogen Wilson Terranes. Overall, our results confirm a high variability in magnetization in the shallower volcanic unit in all areas involved in this inversion, particularly in MM and WR (Figure 6d), as supported by field evidence of strong petrographic variability of rocks (Wörner & Viereck, 1989). In MM, low negative values in magnetization affect almost the whole edifice, interrupted by weakly negative to weakly positive values characterized by a radial pattern retracing that seen in the TMA data. This suggests the reversely-polarized volcanics could reach even the sub-ice topographic surface, interrupted locally by swarms of normally-polarized dikes and lava flows characterized generally by low values of magnetic susceptibility/remanence (see Figure S5 in Supporting Information S1). This hypothesis is corroborated by lower values in the magnetization module and susceptibility shown by normally-polarized rock samples collected in the upper MM (see Table S1 in Supporting Information S1 and references therein). However, such low values could be also due to the influence of the reversely-polarized volcanics below, softening the actual magnetization of normally-polarized dikes and lava flows. Several strong magnetization contrasts are imaged along the entire western flank of MM toward both the northern part and the southern tip, whose values are likely enhanced by the higher slope of that side of MM causing a greater lateral transition between normally- and reversely-polarized volcanics. Moreover, they could be also associated with local intrusion of swarms of normally-polarized dikes. A similar argument applies for WR, where sharp magnetization contrasts are imaged. Regarding the sub-suites OR and SN, they are too small compared to the model resolution to make any consideration. However, as already pointed out, both geochronological and magnetic remanence data corroborate the co-presence of normally- and reversely-polarized volcanic products.

A schematic view of the internal structure of the MVF is given by a 2D forward model (Ghirotto et al., 2021; Talwani & Heirtzler, 1962) performed along a E-W profile shown in Figure 4b, shown and discussed in Figure 7.

As a concluding remark, our models and field magnetic and geochronological data indicate the MVF is constituted by predominant reversely-polarized volcanics forming the main volcanic centers, that are intruded and topped by normally-polarized swarms of dikes and lava flows. The positive anomalies in the TMA dataset, often having radial patterns, would be caused by the magnetization contrast between these oppositely polarized volcanics. Consequently, our results support an older setting in place of the MM stratovolcano, considered in recent studies formed only during the normal-polarity Brunhes epoch (e.g., Giordano et al., 2012).

5. Insights Into the Temporal Evolution of the MVF Complex

Analysis and modeling of our HRAM data, coupled with available magnetic and geochronological field data, have shown the importance of combining geophysical and geological investigations in remote and ice-covered areas. As a result, we have shed light into the inner geophysical and geological structure of the main volcanic centers of the MVF. In addition, here we supply new hints to draw an updated reconstruction of the main volcanic phases that built-up the MVF, proposing an evolutionary model that is more in agreement with those proposed by Wörner and Viereck (1989) and Lanza et al. (1991) rather than that by Giordano et al. (2012). All the discussion is based particularly on the results presented in sub-Section 3.3.

Volcanic activity in MVF is likely to have started at least around the end of the normal polarity Gauss epoch, possibly at WR area (southern MVF) and at other scattered volcanic centers along the eastern coastal area between WR and BR (Figure 8a). The long history of WR is recorded by frequent changes in volcanic products (i.e., pillows, lava flows, hyaloclastites, cinder cones, etc.), reflecting variable deposition conditions (Wörner & Viereck, 1989). At present, the structures and relics of this volcanic phase could be partially hidden either by the ice cover or by further subsequent volcanic deposits and lavas, so we cannot exclude that the actual MM edifice could be characterized in the deeper part by the presence of older volcanic centers (see Figure 8a).

Subsequently to the polarity reversal at the Gauss—Matuyama transition (Figure 8b), first magmatic activity occurred possibly by means of scattered volcanism, generating, e.g., the RH volcanic centers. Afterward, widespread magmatism focused along NW-SE to N-S trending fissures on the crystalline basement of the Ross Orogen Wilson Terrane, from which ENE-WSW trending lava flows established the current reversely-polarized foundation of the entire MVF, developing the bases of the SN, OR, Markham Island, WR and MM volcanic centers.

The normally-polarized volcanics intruding and overlying WR likely started to form during the Olduvai chron, whereas at MM and SN during the subsequent Jaramillo chron (Figure 8b). This phase of volcanic activity might have been driven possibly by the already existent NW-SE to N-S trending fissures, facilitating the intrusion of normally-polarized feeder dikes.

After the last polarity reversal (i.e., Matuyama – Brunhes transition, 0.78 Ma) the volcanic activity, at the beginning still active at the satellite centers of OR and SN, progressively focused on the central and eastern part of the MVF, namely MM, EP and BR inland sector (Figure 8b). In this phase, a new set of NNE-SSW trending faults developed on the eastern side of the field, enhancing volcano-tectonic fracturing between the MM edifice and EP and facilitating the intrusion of swarms of dikes and the deposition of lava flows up to recent times, assuming radial shapes at MM owing to both the filling of radial paleo-valleys and its high topographic gradient.

6. Concluding Remarks

In this paper we have presented the first detailed aeromagnetic study of the MVF, accomplished combining a novel automatic lineament detection method with a two-step magnetic inversion approach, able to shed light into the sub-ice MVF structure and its temporal evolution.

Automatic lineament detection, performed applying the Hough Transform technique on the TDR of TMA data, has revealed the MVF is affected mainly by NW-SE to NNE-SSW structural trends, in good agreement with data from field observations on tectonic structures. TMA data analysis allowed to isolate in the signal two main contributions, that are a large negative long-wavelength and a positive short-wavelength anomaly with radial distribution.

Our two-step magnetic inversion approach, constrained by magnetic property measurements, enabled us to figure out that the geophysical structure of the MVF is constituted by a main reversely-polarized unit superimposed and

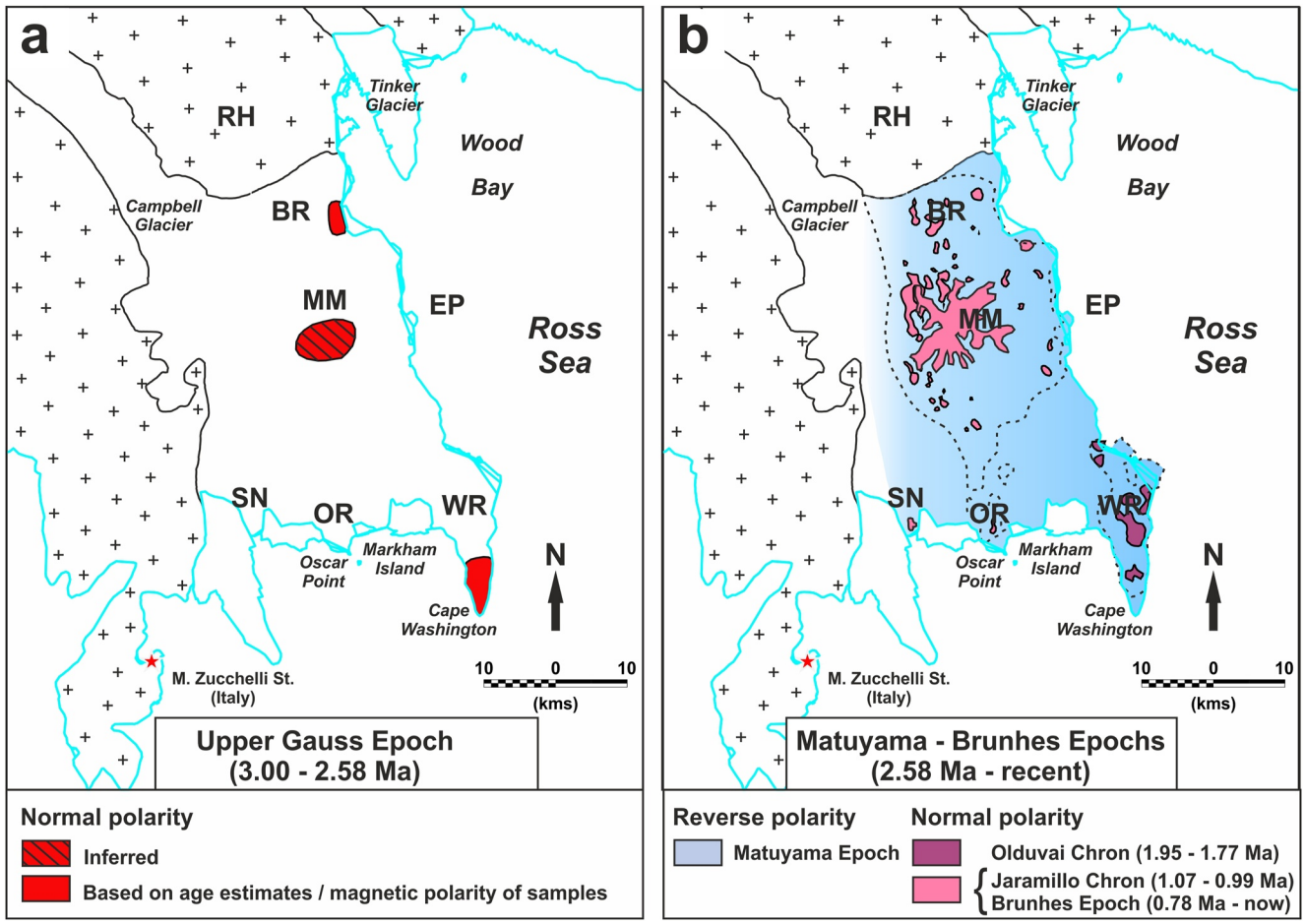

Figure 8. Temporal sequence of the main volcanic phases occurred in MVF. For abbreviations and symbols, see caption of Figure 1. (a) Volcanics formed at the end of the Gauss epoch. Hypothetical ancestral volcanic activity below the MM is based on our inferences, whereas elsewhere is based on age estimates from Kreuzer 1988 (unpubl. Report quoted in Wörner and Viereck (1989)) and Armienti et al. (1991). (b) Volcanic activity occurred in the Matuyama and Brunhes Epochs. For the sake of coherence, the RH sub-suite is not considered since it has been excluded by our modeling. Dashed lines delimit the main sub-suites interested by normal-polarity volcanic activity, particularly MM and WR, as resulted from modeling results. The shape of dikes and lava flows derives from contouring of magnetizations results discussed in sub-Section 4.2 and shown in Figure S5 (Supporting Information S1). The most recent volcanic activity focused on the BR (inland sector), EP and MM sub-suites, in the last assuming a radial shape. The volcanic activity in this period is steered by the activation of the tectonic trend NNE-SSW.

intruded by normally-polarized lava flows and dikes. Field evidence for reversely-polarized volcanics comes from some rock samples collected at the basal slope of MM and in the southern peripheral centers. Normally-polarized volcanic flows would locally overlie the reversely-polarized basal unit on the main volcanic centers WR, SN, OR, EP, MM, and BR, assuming radial shapes both on the MM edifice and WR possibly due to paleo-channels excavated in the reversely-polarized basal unit. In addition, the MM stratovolcano appears internally affected by swarms of feeder dikes as a consequence of the longer magmatic activity occurring in this part of the MVF.

Combining our results with available geochronological information from rocks samples collected in the field, we suggest for the MVF a geological history more complex in respect to what was thought so far. In our reconstruction, widespread magmatic activity would have started at least at the reverse polarity Matuyama epoch also at MM, driven by NW-SE to N-S fractures on the crystalline basement of the Ross Orogen Wilson Terrane. However, scattered volcanic activity in the northeastern peripheral center of BR and in the southern tip of WR could have begun even at the end of the normal polarity Gauss epoch. After the last magnetic polarity reversal, volcanic activity progressively moved toward the central portion of the MVF, focusing on the last hundreds/tens of thousands of years on MM and EP. The most recent phase of volcanic activity was driven by a new NNE-SSW trending fault set, reflecting likely an activation of major extensional fault zones along the current coastline (Vignaroli et al., 2015).

Data Availability Statement

The datasets and models discussed in the manuscript are provided at a Zenodo open access repository (Ghirotto et al., 2022, https://doi.org/10.5281/zenodo.7099500), or upon request addressed to the corresponding author.

Acknowledgments
This work was supported by the projects TIMM (PNRA – 2002/3.11) and BOOST (PNRA19_00051 – A1), funded by the Italian Antarctic research program (PNRA), and partially by the University of Genova (Fondi di Ricerca di Ateneo – FRA 2020). The authors gratefully thank Richard Blakely, Richard Saltus, Gerhard Wörner and an anonymous reviewer for the valuable comments and suggestions provided to improve this work. A.G. would like to acknowledge the Dipartimento di Scienze della Terra, dell'Ambiente e della Vita (DISTAV) of the University of Genova for the further financial and material support provided in the context of his PhD program.

References

Adamson, R. G., & Cavaney, R. J. (1967). Volcanic debris-layers near mount Melbourne, northern Victoria Land, Antarctica. *New Zealand Journal of Geology and Geophysics*, *10*(2), 418–421. https://doi.org/10.1080/00288306.1967.10426745

Armadillo, E., Bozzo, E., Gambetta, M., & Rizzello, D. (2012). Impact of human activities on the geomagnetic field of Antarctica: A high resolution aeromagnetic survey over Mario Zucchelli station. *Environment International*, *47*, 1–7. https://doi.org/10.1016/j.envint.2012.05.005

Armadillo, E., Ferraccioli, F., Zunino, A., Bozzo, E., Rocchi, S., Armienti, P., *et al.* (2007). Aeromagnetic search for Cenozoic magmatism over the admiralty mountains block (East Antarctica). In A. K. Cooper (Ed.), *Antarctica: A keystone in a changing world–online proceedings of the 10th ISAES* (pp. 1–4). USGS Open-File Report.

Armienti, P., & Baroni, C. (1999). Cenozoic climatic change in Antarctica recorded by volcanic activity and landscape evolution. *Geology*, *27*(7), 617–620. https://doi.org/10.1130/0091-7613(1999)027<0617:ccciar>2.3.co;2

Armienti, P., Civetta, L., Innocenti, F., Manetti, P., & Tripodo, A. (1991). New petrological and geochemical data on Mt. Melbourne volcanic field, northern Victoria Land, Antarctica. (II Italian Antarctic expedition). *Memorie della Societa Geologica Italiana*(46), 397–424.

Armienti, P., Ghezzo, C., Innocenti, F., Manetti, P., Rocchi, S., & Tonarini, S. (1988). Palaeozoic and Cainozoic intrusives of Wilson Terrane: Geochemical and isotopic data. *Memorie della Societa Geologica Italiana*, *43*, 67–75.

Armstrong, R. L. (1978). K-Ar dating: Late Cenozoic McMurdo volcanic group and dry valley glacial history, Victoria Land, Antarctica. *New Zealand Journal of Geology and Geophysics*, *21*(6), 685–698. https://doi.org/10.1080/00288306.1978.10425199

Beccaluva, L., Civetta, L., Coltorti, M., Orsi, G., Saccani, E., & Siena, F. (1991). Basanite to tephrite lavas from Melbourne volcanic province, Victoria Land, Antarctica. *Memorie della Societa Geologica Italiana*(46), 383–395.

Beccaluva, L., Coltorti, M., Orsi, G., Saccani, E., & Siena, F. (1991). Nature and evolution of the sub-continental lithospheric mantle of Antarctica: Evidence from ultramafic xenoliths of the Melbourne volcanic province (northern Victoria Land, Antarctica). *Memorie della Societa Geologica Italiana*(46), 353–370.

Bhattacharyya, B. K. (1964). Magnetic anomalies due to prism-shaped bodies with arbitrary polarization. *Geophysics*, *29*(4), 517–531. https://doi.org/10.1190/1.1439386

Bindschadler, R., Vornberger, P., Fleming, A., Fox, A., Mullins, J., Binnie, D., et al. (2008). The Landsat image mosaic of Antarctica. *Remote Sensing of Environment*, *112*(12), 4214–4226. https://doi.org/10.1016/j.rse.2008.07.006

Blakely, R. J. (1996). *Potential theory in gravity and magnetic applications*. Cambridge University Press.

Blanco-Montenegro, I., Montesinos, F. G., & Arnoso, J. (2018). Aeromagnetic anomalies reveal the link between magmatism and tectonics during the early formation of the Canary Islands. *Scientific Reports*, *8*(1), 1–14. https://doi.org/10.1038/s41598-017-18813-w

Bonaccorso, A., Falzone, G., Gambino, S., & Villari, L. (1995). Tilt signals recorded at Mt Melbourne volcano (northern Victoria Land, Antarctica) between 1989–94. *Terra Antartica*, *2*(2), 111–116.

Bonaccorso, A. S. G. E. A., Gambino, S., Falzone, G., & Privitera, E. (1996). Physics volcanological studies in the activity framework of the Mt. Melbourne Observatory (northern Victoria Land, Antarctica). *Italian Geophysical Observatories in Antarctica, Editrice Compositori*, *67*, 92.

Bouligand, C., Glen, J. M., & Blakely, R. J. (2014). Distribution of buried hydrothermal alteration deduced from high-resolution magnetic surveys in Yellowstone National Park. *Journal of Geophysical Research: Solid Earth*, *119*(4), 2595–2630. https://doi.org/10.1002/2013jb010802

Bozzo, E., Caneva, G., & Manzoni, M. (1987). *Geomagnetic investigations in the Terra Nova Bay region, Victoria Land, Antarctica*. 5th Symp. Antarctica Earth Science, Cambridge 1987, Abstracts, 143.

Bozzo, E., Ghezzi, G., Simeoni, U., & Taviani, M. (1991). The magnetic susceptibility of Ross Sea continental shelf surficial sediments (Antarctica). *Memorie della Societa Geologica Italiana*(46), 563–569.

Cande, S. C., & Kent, D. V. (1992). A new geomagnetic polarity time scale for the Late Cretaceous and Cenozoic. *Journal of Geophysical Research*, *97*(B10), 13917–13951. https://doi.org/10.1029/92jb01202

Cande, S. C., & Kent, D. V. (1995). Revised calibration of the geomagnetic polarity timescale for the Late Cretaceous and Cenozoic. *Journal of Geophysical Research*, *100*(B4), 6093–6095. https://doi.org/10.1029/94jb03098

Carmignani, L., Ghezzo, C., Gosso, G., Lombardo, B., Meccheri, M., Montrasio, A., et al. (1987). Geological map of the area between David and Mariner glaciers, Victoria Land, Antarctica. *Memorie Societa Geologica Italiana*, *33*. Geologic map.

Clark, D. A. (1997). Magnetic petrophysics and magnetic petrology: Aids to geological interpretation of magnetic surveys. *AGSO Journal of Australian Geology and Geophysics*, *17*(2), 83–103.

Cremisini, C., Gianelli, G., Mussi, M., & Torcini, S. (1991). Geochemistry and isotope chemistry of surface waters and geothermal manifestations at Terra Nova Bay, (Victoria Land, Antarctica). *Memorie della Societa Geologica Italiana*(46), 463–475.

Damaske, D., Schreckenberger, B., & Goldmann, F. (2014). A high resolution aeromagnetic survey over the Mesa Range, northern Victoria Land, Antarctica. *herausgegeben vom Alfred-Wegener-Institut Helmholtz-Zentrum für Polar-und Meeresforschung und der Deutschen Gesellschaft für Polarforschung e. V.*, *84*(1), 1–13.

Del Carlo, P., Di Roberto, A., Di Vincenzo, G., Re, G., Albert, P. G., Nazzari, M., et al. (2022). Tephrostratigraphy of proximal pyroclastic sequences at Mount Melbourne (northern Victoria Land, Antarctica): Insights into the volcanic activity since the last glacial period. *Journal of Volcanology and Geothermal Research*, *422*, 107457. https://doi.org/10.1016/j.jvolgeores.2021.107457

Duda, R. O., & Hart, P. E. (1972). Use of the Hough transformation to detect lines and curves in pictures. *Communications of the ACM*, *15*(1), 11–15. https://doi.org/10.1145/361237.361242

Dumont, M., Reninger, P. A., Aunay, B., Pryet, A., Jougnot, D., Join, J. L., et al. (2021). Hydrogeophysical characterization in a volcanic context from local to regional scales combining airborne electromagnetism and magnetism. *Geophysical Research Letters*, *48*(12), e2020GL092000. https://doi.org/10.1029/2020gl092000

Ebbing, J., Dilixiati, Y., Haas, P., Ferraccioli, F., & Scheiber-Enslin, S. (2021). East Antarctica magnetically linked to its ancient neighbours in Gondwana. *Scientific Reports*, *11*(1), 1–11. https://doi.org/10.1038/s41598-021-84834-1

Fairhead, J. D. (2016). *Advances in gravity and magnetic processing and interpretation*. EAGE Publications.

Ferraccioli, F., Armadillo, E., Bozzo, E., & Privitera, E. (2000). Magnetics and gravity image tectonic framework of the Mount Melbourne Volcano area (Antarctica). *Physics and Chemistry of the Earth - Part A: Solid Earth and Geodesy*, *25*(4), 387–393. https://doi.org/10.1016/s1464-1895(00)00061-2

Ferraccioli, F., Armadillo, E., Jordan, T., Bozzo, E., & Corr, H. (2009a). Aeromagnetic exploration over the East Antarctic ice sheet: A new view of the Wilkes subglacial basin. *Tectonophysics*, *478*(1–2), 62–77. https://doi.org/10.1016/j.tecto.2009.03.013

Ferraccioli, F., Armadillo, E., Zunino, A., Bozzo, E., Rocchi, S., & Armienti, P. (2009b). Magmatic and tectonic patterns over the Northern Victoria Land sector of the Transantarctic Mountains from new aeromagnetic imaging. *Tectonophysics*, *478*(1–2), 43–61. https://doi.org/10.1016/j.tecto.2008.11.028

Ferraccioli, F., Gambetta, M., & Bozzo, E. (1998). Microlevelling procedures applied to regional aeromagnetic data: An example from the Transantarctic Mountains (Antarctica). *Geophysical Prospecting*, *46*, 177–196. https://doi.org/10.1046/j.1365-2478.1998.00080.x

Ferraccioli, F., Jones, P. C., Curtis, M. L., Leat, P. T., & Riley, T. R. (2005). Tectonic and magmatic patterns in the Jutulstraumen rift (?) region, East Antarctica, as imaged by high-resolution aeromagnetic data. *Earth Planets and Space*, *57*(8), 767–780. https://doi.org/10.1186/bf03351856

Finn, C. A., Bedrosian, P. A., Holbrook, W. S., Auken, E., Bloss, B. R., & Crosbie, J. (2022). Geophysical imaging of the Yellowstone hydrothermal plumbing system. *Nature*, *603*(7902), 643–647. https://doi.org/10.1038/s41586-021-04379-1

Finn, C. A., Deszcz-Pan, M., Anderson, E. D., & John, D. A. (2007). Three-dimensional geophysical mapping of rock alteration and water content at Mount Adams, Washington: Implications for lahar hazards. *Journal of Geophysical Research*, *112*(B10). https://doi.org/10.1029/2006jb004783

Finn, C. A., & Morgan, L. A. (2002). High-resolution aeromagnetic mapping of volcanic terrain, Yellowstone National Park. *Journal of Volcanology and Geothermal Research*, *115*(1–2), 207–231. https://doi.org/10.1016/s0377-0273(01)00317-1

Gambino, S., Aloisi, M., Falzone, G., & Ferro, A. (2016). Tilt signals at Mount Melbourne, Antarctica: Evidence of a shallow volcanic source. *Polar Research*, *35*(1), 28269. https://doi.org/10.3402/polar.v35.28269

Gambino, S., Armienti, P., Cannata, A., Del Carlo, P., Giudice, G., Giuffrida, G., et al. (2021). Mount Melbourne and Mount Rittmann. *Geological Society, London, Memoirs*, *55*(1), 741–758.

GANOVEX. (1987). Geological map of north Victoria Land, Antarctica, 1:500000. Explanatory notes. German Antarctic north Victoria Land expedition 1982/83. *Geologisches Jahrbuch*, *2*, 7–79.III

Geshi, N. (2008). Vertical and lateral propagation of radial dikes inferred from the flow-direction analysis of the radial dike swarm in Komochi Volcano, Central Japan. *Journal of Volcanology and Geothermal Research*, *173*(1–2), 122–134. https://doi.org/10.1016/j.jvolgeores.2008.01.001

Ghidella, M. E., Zambrano, O. M., Ferraccioli, F., Lirio, J. M., Zakrajsek, A. F., Ferris, J., & Jordan, T. A. (2013). Analysis of James Ross Island volcanic complex and sedimentary basin based on high-resolution aeromagnetic data. *Tectonophysics*, *585*, 90–101. https://doi.org/10.1016/j.tecto.2012.06.039

Ghirotto, A., Armadillo, E., Crispini, L., Zunino, A., Caratori Tontini, F., & Ferraccioli, F. (2022). Datasets and models about the geophysical characterization of the Mt. Melbourne volcanic field (Northern Victoria Land, Antarctica). *Zenodo*. https://doi.org/10.5281/zenodo.7099500

Ghirotto, A., Zunino, A., Armadillo, E., & Mosegaard, K. (2021). Magnetic anomalies caused by 2D polygonal structures with uniform arbitrary polarization: New insights from analytical/numerical comparison among available algorithm formulations. *Geophysical Research Letters*, *48*(7), e2020GL091732. https://doi.org/10.1029/2020gl091732

Giordano, G., Lucci, F., Phillips, D., Cozzupoli, D., & Runci, V. (2012). Stratigraphy, geochronology and evolution of the Mt. Melbourne volcanic field (North Victoria Land, Antarctica). *Bulletin of Volcanology*, *74*(9), 1985–2005. https://doi.org/10.1007/s00445-012-0643-8

Golynsky, A. V., Ferraccioli, F., Hong, J. K., Golynsky, D. A., Von Frese, R. R. B., Young, D. A., et al. (2018). New magnetic anomaly map of the Antarctic. *Geophysical Research Letters*, *45*(13), 6437–6449. https://doi.org/10.1029/2018gl078153

Goodge, J. W., & Finn, C. A. (2010). Glimpses of East Antarctica: Aeromagnetic and satellite magnetic view from the central transantarctic mountains of East Antarctica. *Journal of Geophysical Research*, *115*(B9). https://doi.org/10.1029/2009jb006890

Grant, F. S. (1973). *Magnetic susceptibility mapping: The first year's experience: In 43rd Annual International Meeting*. Society of Exploration Geophysics.

Gubellini, A., & Postpischl, D. (1991). The Mount Melbourne (Antarctica) geodetic network. *Memorie della Societa Geologica Italiana*(46), 595–610.

Harrington, H. J. (1958). Nomenclature of rock units in the Ross Sea region, Antarctica. *Nature*, *182*(4361), 290–291. https://doi.org/10.1038/182290a0

Hart, P. E. (2009). How the Hough transform was invented [DSP History]. *IEEE Signal Processing Magazine*, *26*(6), 18–22. https://doi.org/10.1109/msp.2009.934181

Hinze, W. J., Von Frese, R. R., Von Frese, R., & Saad, A. H. (2013). *Gravity and magnetic exploration: Principles, practices, and applications*. Cambridge University Press.

Hörnig, I., Wörner, G., & Zipfel, J. (1991). Lower crustal and mantle xenoliths from the Mt. Melbourne volcanic field, northern Victoria Land, Antarctica. *Memorie della Societa Geologica Italiana*(46), 337–352.

Hrouda, F. (1982). Magnetic anisotropy of rocks and its application in geology and geophysics. *Geophysical Surveys*, *5*(1), 37–82. https://doi.org/10.1007/bf01450244

Jordan, T. A., Ferraccioli, F., & Forsberg, R. (2022). An embayment in the East Antarctic basement constrains the shape of the Rodinian continental margin. *Communications Earth & Environment*, *3*(1), 1–8. https://doi.org/10.1038/s43247-022-00375-z

Jordan, T. A., Neale, R. F., Leat, P. T., Vaughan, A. P. M., Flowerdew, M. J., Riley, T. R., et al. (2014). Structure and evolution of Cenozoic arc magmatism on the Antarctic Peninsula: A high resolution aeromagnetic perspective. *Geophysical Journal International*, *198*(3), 1758–1774. https://doi.org/10.1093/gji/ggu233

Keys, J. R., McIntosh, W. C., & Kyle, P. R. (1983). Volcanic activity of mount Melbourne, northern Victoria Land. *Antarctic Journal of the United States*, *18*(5), 10–11.

Kim, H. R., Golynsky, A. V., Golynsky, D. A., Yu, H., Von Frese, R. R. B., & Hong, J. K. (2022). New magnetic anomaly constraints on the Antarctic Crust. *Journal of Geophysical Research: Solid Earth*, *127*(3), e2021JB023329. https://doi.org/10.1029/2021jb023329

Kovesi, P. (1999). Image features from phase congruency. *Videre: A Journal of Computer Vision Research*, *1*(3), 1–26.

Kovesi, P. (2003). Phase congruency detects corners and edges. In *The Australian pattern recognition society conference: Digital image computing: Techniques and applications* (pp. 309–318).

Kyle, P. R. (1990). A.ll. Melbourne Province. In W. E. LeMasurier & J. W. Thomson (Eds.), *Volcanoes of the Antarctic plate and southern oceans* (Vol. 48, pp. 48–53). AGU, Antarctic Research Series.

Kyle, P. R., & Cole, J. W. (1974). Structural control of volcanism in the McMurdo volcanic group, Antarctica. *Bulletin Volcanologique*, *38*(1), 16–25. https://doi.org/10.1007/bf02597798

Lanza, R., Manzoni, M., & Miletto, M. (1991). Paleomagnetic data from the Mt. Melbourne volcanic province, north Victoria Land, Antarctica. *Memorie della Societa Geologica Italiana*(46), 533–541.

Lanzafame, G., & Villari, L. (1991). Structural evolution and volcanism in northern Victoria Land (Antarctica): Data from Mt. Melbourne-Mt. Overlord-Malta plateau region. *Memorie della Societa Geologica Italiana*(46), 371–381.
Läufer, A. L., Damaske, D., & Lisker, F. (2011). Neogene tectonics in the Edisto and Tucker Inlet region and its correlation with offshore magnetic anomalies north of Cape Adare, northern Victoria Land, Antarctica. *Polarforschung*, *80*(2), 111–126.
Lee, H., Seo, H., Han, H., Ju, H., & Lee, J. (2021). Velocity anomaly of Campbell Glacier, East Antarctica, observed by Double-differential Interferometric SAR and ice penetrating radar. *Remote Sensing*, *13*(14), 2691. https://doi.org/10.3390/rs13142691
Lee, M. J., Kyle, P. R., Iverson, N. A., Lee, J. I., & Han, Y. (2019). Rittmann volcano, Antarctica as the source of a widespread 1252±2 CE tephra layer in Antarctica ice. *Earth and Planetary Science Letters*, *521*, 169–176. https://doi.org/10.1016/j.epsl.2019.06.002
Lee, M. J., Lee, J. I., Kim, T. H., Lee, J., & Nagao, K. (2015). Age, geochemistry and Sr-Nd-Pb isotopic compositions of alkali volcanic rocks from Mt. Melbourne and the Western Ross Sea, Antarctica. *Geosciences Journal*, *19*(4), 681–695. https://doi.org/10.1007/s12303-015-0061-y
Lee, T. C., Kashyap, R. L., & Chu, C. N. (1994). Building skeleton models via 3-D medial surface axis thinning algorithms. *CVGIP: Graphical Models and Image Processing*, *56*(6), 462–478. https://doi.org/10.1006/cgip.1994.1042
Luyendyk, A. P. J. (1997). Processing of airborne magnetic data. *AGSO Journal of Australian Geology and Geophysics*, *17*, 31–38.
Lyon, G. L. (1986). Stable isotope stratigraphy of ice cores and the age of the last eruption at Mount Melbourne, Antarctica. *New Zealand Journal of Geology and Geophysics*, *29*(1), 135–138. https://doi.org/10.1080/00288306.1986.10427528
Lyon, G. L., & Giggenbach, W. F. (1974). Geothermal activity in Victoria Land, Antarctica. *New Zealand Journal of Geology and Geophysics*, *17*(3), 511–521. https://doi.org/10.1080/00288306.1973.10421578
Mader, G. L. (1992). Rapid static and kinematic global positioning system solutions using the ambiguity function technique. *Journal of Geophysical Research*, *97*(B3), 3271–3283. https://doi.org/10.1029/91jb02845
Manzoni, M., & Miletto, M. (1988). Rock-magnetic properties of volcanites from Mt. Melbourne (north Victoria Land): Preliminary results. *Memorie della Societa Geologica Italiana*, *43*, 173–180.
Martelet, G., Reninger, P. A., Perrin, J., & Deparis, J. (2014). Acquisition géophysique héliportée de l'île de La Réunion (Report). BRGM. BRGM/RP-63818-FR, p. 91. Retrieved from https://infoterre.brgm.fr/rapports/RP-63818-FR.pdf
Mieth, M., Jacobs, J., Ruppel, A., Damaske, D., Läufer, A., & Jokat, W. (2014). New detailed aeromagnetic and geological data of eastern Dronning Maud Land: Implications for refining the tectonic and structural framework of Sør Rondane, East Antarctica. *Precambrian Research*, *245*, 174–185. https://doi.org/10.1016/j.precamres.2014.02.009
Miller, H. G., & Singh, V. (1994). Potential field tilt—A new concept for location of potential field sources. *Journal of Applied Geophysics*, *32*(2–3), 213–217. https://doi.org/10.1016/0926-9851(94)90022-1
Morlighem, M., Rignot, E., Binder, T., Blankenship, D., Drews, R., Eagles, G., et al. (2020). Deep glacial troughs and stabilizing ridges unveiled beneath the margins of the Antarctic ice sheet. *Nature Geoscience*, *13*, 132–137. https://doi.org/10.1038/s41561-019-0510-8
Müller, P., Schmidt-Thomé, M., Kreuzer, H., Tessensohn, F., & Vetter, U. (1991). Cenozoic peralkaline magmatism at the Western margin of the Ross Sea, Antarctica. *Memorie della Societa Geologica Italiana*(46), 315–336.
Nathan, S., & Schulte, F. J. (1967). Recent thermal and volcanic activity on mount Melbourne, northern Victoria Land, Antarctica. *New Zealand Journal of Geology and Geophysics*, *10*(2), 422–430. https://doi.org/10.1080/00288306.1967.10426746
Nathan, S., & Schulte, F. J. (1968). Geology and petrology of the Campbell—Aviator Divide, northern Victoria Land, Antarctica: Part 1—Post Paleozoic rocks. *New Zealand Journal of Geology and Geophysics*, *11*(4), 940–975. https://doi.org/10.1080/00288306.1968.10420762
O'gorman, F., & Clowes, M. B. (1976). Finding picture edges through collinearity of feature points. *IEEE Transactions on Computers*, *25*(04), 449–456. https://doi.org/10.1109/tc.1976.1674627
Oldenburg, D. W. (1974). The inversion and interpretation of gravity anomalies. *Geophysics*, *39*(4), 526–536. https://doi.org/10.1190/1.1440444
Parker, R. L. (1972). The rapid calculation of potential anomalies. *Geophysical Journal of the Royal Astronomical Society*, *42*, 315–334.
Pasquale, V., Verdoya, M., Chiozzi, P., & Armadillo, E. (2009). Thermal, radioactive and magnetic properties of the lavas of the Mt Melbourne volcanic field (Victoria Land, Antarctica). *Annals of Geophysics*, *52*(2), 197–207.
Pertusati, P. C., Musumeci, G., Carosi, R., Meccheri, M., Baroni, C., Capponi, G., et al. (2012). *Antarctic geological 1: 250.000 map Series–Mount Melbourne Quadrangle (Victoria Land), GIGAMAP*. MIUR-PNRA.
Rocchi, S., Armienti, P., D'Orazio, M., Tonarini, S., Wijbrans, J. R., & Di Vincenzo, G. (2002). Cenozoic magmatism in the Western Ross embayment: Role of mantle plume versus plate dynamics in the development of the West Antarctic Rift System. *Journal of Geophysical Research*, *107*(B9), ECV5. https://doi.org/10.1029/2001jb000515
Roland, N. W., & Tessensohn, F. (1987). Rennick faulting-an early phase of Ross Sea rifting. *Geologisches Jahrbuch. Reihe B, Regionale Geologie Ausland*(66), 203–229.
Ruppel, A., Läufer, A., Crispini, L., Capponi, G., & Lisker, F. (2017). April). A high-resolution aeromagnetic survey over the Lanterman Range, northern Victoria Land, Antarctica. *EGU General Assembly Conference Abstracts*, 14182.
Salem, A., Williams, S., Fairhead, J. D., Ravat, D., & Smith, R. (2007). Tilt-depth method: A simple depth estimation method using first-order magnetic derivatives. *The Leading Edge*, *26*(12), 1502–1505. https://doi.org/10.1190/1.2821934
Salvini, F., Brancolini, G., Busetti, M., Storti, F., Mazzarini, F., & Coren, F. (1997). Cenozoic geodynamics of the Ross Sea region, Antarctica: Crustal extension, intraplate strike-slip faulting, and tectonic inheritance. *Journal of Geophysical Research*, *102*(B11), 24669–24696. https://doi.org/10.1029/97jb01643
Silva, J. B., & Hohmann, G. W. (1984). Airborne magnetic susceptibility mapping. *Exploration Geophysics*, *15*(1), 1–13. https://doi.org/10.1071/eg984001
Smellie, J. L., & Rocchi, S. (2021). Northern Victoria Land: Volcanology. *Geological Society, Memoirs*, *55*(1), 347–381. https://doi.org/10.1144/m55-2018-60
Storti, F., Balestrieri, M. L., Balsamo, F., & Rossetti, F. (2008). Structural and thermochronological constraints to the evolution of the West Antarctic Rift System in central Victoria Land. *Tectonics*, *27*(4), a–n. https://doi.org/10.1029/2006TC002066
Talarico, F., Armadillo, E., Ferraccioli, F., & Rastelli, N. (2003). Magnetic petrology of the Ross Orogen in Oates Land (Antarctica). *Terra Antartica*, *10*, 197–220.
Talwani, M., & Heirtzler, J. R. (1962). The mathematical expression for the magnetic anomaly over a two-dimensional body of polygonal cross-section. *Lamont. Doherty Geol. Obs. Columbia Univ., Tech. Rep*, *6*.
Tarantola, A. (2005). *Inverse problem theory and methods for model parameter estimation*. Society for Industrial and Applied Mathematics.
Tarling, D. & Hrouda, F. (Eds.) (1993)., *Magnetic anisotropy of rocks*. Springer Science & Business Media.
Tonarini, S., Rocchi, S., Armienti, P., & Innocenti, F. (1997). Constraints on timing of Ross Sea rifting inferred from Cenozoic intrusions from northern Victoria Land, Antarctica. In C. A. Ricci (Ed.), *The Antarctic region: Geological evolution and processes* (pp. 511–521). Terra Antarctica publication.

Verduzco, B., Fairhead, J. D., Green, C. M., & MacKenzie, C. (2004). New insights into magnetic derivatives for structural mapping. *The Leading Edge*, *23*(2), 116–119. https://doi.org/10.1190/1.1651454

Vignaroli, G., Balsamo, F., Giordano, G., Rossetti, F., & Storti, F. (2015). Miocene-to-Quaternary oblique rifting signature in the Western Ross Sea from fault patterns in the McMurdo volcanic group, north Victoria Land, Antarctica. *Tectonophysics*, *656*, 74–90. https://doi.org/10.1016/j.tecto.2015.05.027

Wilson, G., Damaske, D., Möller, H. D., Tinto, K., & Jordan, T. (2007). The geological evolution of southern McMurdo Sound-new evidence from a high-resolution aeromagnetic survey. *Geophysical Journal International*, *170*(1), 93–100. https://doi.org/10.1111/j.1365-246x.2007.03395.x

Wörner, G., & Viereck, L. (1987). Subglacial to emergent volcanism at Shield Nunatak, Mt. Melbourne volcanic field, Antarctica. *Polarforschung*, *57*(1/2), 27–41.

Wörner, G., & Viereck, L. (1989). The Mt. Melbourne volcanic field (Victoria Land, Antarctica). I: Field observations. *Geologisches Jahrbuch. Reihe E, Geophysik*(38), 369–393.

Wörner, G., Viereck, L., Hertogen, J., & Niephaus, H. (1989). The Mt. Melbourne volcanic field (Victoria Land, Antartica). II. Geochemistry and magma genesis. *Geologisches Jahrbuch. Reihe E, Geophysik*(38), 395–433.

Zunino, A., Benvenuto, F., Armadillo, E., Bertero, M., & Bozzo, E. (2009). Iterative deconvolution and semiblind deconvolution methods in magnetic archaeological prospecting. *Geophysics*, *74*(4), L43–L51. https://doi.org/10.1190/1.3129263